

The REBELS ALMA Survey: cosmic dust temperature evolution out to $z \sim 7$

L. Sommovigo^{1*}, A. Ferrara¹, A. Pallottini¹, P. Dayal², R.J. Bouwens³, R. Smit⁴, E. da Cunha^{5,6b}, I. De Looze^{7,8}, R. A. A. Bowler⁹, J. Hodge³, H. Inami¹⁰, P. Oesch^{11,12}, R. Endsley¹³, V. Gonzalez^{14,15}, S. Schouws³, D. Stark¹³, M. Stefanon³, M. Aravena¹⁶, L. Graziani^{17,18}, D. Riechers¹⁹, R. Schneider^{17,20}, P. van der Werf³, H. Algera¹⁰, L. Barrufet¹¹, Y. Fudamoto^{11,21,22}, A. P. S. Hygate³, I. Labbé²³, Y. Li^{24,25}, T. Nanayakkara²³, M. Topping¹³

¹ Scuola Normale Superiore, Piazza dei Cavalieri 7, I-56126 Pisa, Italy

² Kapteyn Astronomical Institute, University of Groningen, 9700 AV Groningen, The Netherlands

³ Leiden Observatory, Leiden University, NL-2300 RA Leiden, Netherlands

⁴ Astrophysics Research Institute, Liverpool John Moores University, 146 Brownlow Hill, Liverpool L3 5RF, United Kingdom

⁵ International Centre for Radio Astronomy Research, University of Western Australia, 35 Stirling Hwy, Crawley, 26WA 6009, Australia

⁶ ARC Centre of Excellence for All Sky Astrophysics in 3 Dimensions (ASTRO 3D), Australia

⁷ Sterrenkundig Observatorium, Ghent University, Krijgslaan 281 - S9, 9000 Gent, Belgium

⁸ Dept. of Physics & Astronomy, University College London, Gower Street, London WC1E 6BT, United Kingdom

⁹ Astrophysics, The Denys Wilkinson Building, University of Oxford, Keble Road, Oxford, OX1 3RH, United Kingdom

¹⁰ Hiroshima Astrophysical Science Center, Hiroshima University, 1-3-1 Kagamiyama, Higashi-Hiroshima, Hiroshima 739-8526, Japan

¹¹ Observatoire de Genève, 1290 Versoix, Switzerland

¹² Cosmic Dawn Center (DAWN), Niels Bohr Institute, University of Copenhagen, Jagtvej 128, København N, DK-2200, Denmark

¹³ Steward Observatory, University of Arizona, 933 N Cherry Ave, Tucson, AZ 85721, United States

¹⁴ Departamento de Astronomía, Universidad de Chile, Casilla 36-D, Santiago 7591245, Chile

¹⁵ Centro de Astrofísica y Tecnologías Afines (CATA), Camino del Observatorio 1515, Las Condes, Santiago, 7591245, Chile

¹⁶ Nucleo de Astronomía, Facultad de Ingeniería y Ciencias, Universidad Diego Portales, Av. Ejército 441, Santiago, Chile

¹⁷ Dipartimento di Fisica, Sapienza, Università di Roma, Piazzale Aldo Moro 5, I-00185 Roma, Italy

¹⁸ INAF/Osservatorio Astrofisico di Arcetri, Largo E. Fermi 5, I-50125 Firenze, Italy

¹⁹ I. Physikalisches Institut, Universität zu Köln, Zùlpicher Strasse 77, D-50937 Köln, Germany

²⁰ INAF/Osservatorio Astronomico di Roma, via Frascati 33, 00078 Monte Porzio Catone, Roma, Italy

²¹ Research Institute for Science and Engineering, Waseda University, 3-4-1 Okubo, Shinjuku, Tokyo 169-8555, Japan

²² National Astronomical Observatory of Japan, 2-21-1, Osawa, Mitaka, Tokyo, Japan

²³ Centre for Astrophysics & Supercomputing, Swinburne University of Technology, PO Box 218, Hawthorn, VIC 3112, Australia

²⁴ Department of Astronomy & Astrophysics, The Pennsylvania State University, 525 Davey Lab, University Park, PA 16802, USA

²⁵ Institute for Gravitation and the Cosmos, The Pennsylvania State University, University Park, PA 16802, USA

4 February 2022

ABSTRACT

ALMA observations have revealed the presence of dust in the first generations of galaxies in the Universe. However, the dust temperature T_d remains mostly unconstrained due to the few available FIR continuum data at redshift $z > 5$. This introduces large uncertainties in several properties of high- z galaxies, namely their dust masses, infrared luminosities, and obscured fraction of star formation. Using a new method based on simultaneous [C II] $158\mu\text{m}$ line and underlying dust continuum measurements, we derive T_d in the continuum and [C II] detected $z \approx 7$ galaxies in the ALMA Large Project REBELS sample. We find $39\text{ K} < T_d < 58\text{ K}$, and dust masses in the narrow range $M_d = (0.9 - 3.6) \times 10^7 M_\odot$. These results allow us to extend for the first time the reported $T_d(z)$ relation into the Epoch of Reionization. We produce a *new physical model* that explains the increasing $T_d(z)$ trend with the decrease of gas depletion time, $t_{\text{dep}} = M_g/\text{SFR}$, induced by the higher cosmological accretion rate at early times; this hypothesis yields $T_d \propto (1+z)^{0.4}$. The model also explains the observed T_d scatter at a fixed redshift. We find that dust is warmer in obscured sources, as a larger obscuration results in more efficient dust heating. For UV-transparent (obscured) galaxies, T_d only depends on the gas column density (metallicity), $T_d \propto N_H^{1/6}$ ($T_d \propto Z^{-1/6}$). REBELS galaxies are on average relatively transparent, with effective gas column densities around $N_H \approx (0.03 - 1) \times 10^{21}\text{cm}^{-2}$. We predict that other high- z galaxies (e.g. MACS0416-Y1, A2744-YD4), with estimated $T_d \gg 60\text{ K}$, are significantly obscured, low-metallicity systems. In fact T_d is higher in metal-poor systems due to their smaller dust content, which for fixed L_{IR} results in warmer temperatures.

Key words: galaxies: high-redshift, infrared: ISM, ISM: dust, extinction, methods: analytical – data analysis

1 INTRODUCTION

The rest-frame Ultraviolet (UV) emission from galaxies in the Epoch of Reionization (EoR) has been extensively studied thanks to the Hubble Space Telescope (HST) and ground-based telescopes (for UV luminosity functions see: Bradley et al. 2012; Oesch et al. 2013; McLure et al. 2013; Bowler et al. 2015; Atek et al. 2015; Bouwens et al. 2015; Livermore et al. 2017, for single detections see: Bouwens et al. 2010, 2011; Ellis et al. 2012; Bradley et al. 2014; Oesch et al. 2016).

Recently, also the Far-Infrared (FIR) emission from such early sources has become observable thanks to the advent of high sensitivity millimetre interferometers such as the Atacama Large Millimeter Array (for surveys see: Capak et al. 2015; Carilli et al. 2016; Bouwens et al. 2016; Barisic et al. 2017; Bowler et al. 2018; Bethermin et al. 2020; Schaerer et al. 2020, for comprehensive reviews see: Carilli & Walter 2013; Dunlop 2016). The combination of data from these different instruments has allowed us to glimpse the interstellar medium (ISM) of early galaxies (see e.g. Dunlop et al. 2013; Stark 2016; Dayal & Ferrara 2018; Hodge & da Cunha 2020) for the first time.

The FIR emission from galaxies includes FIR lines, arising from atomic and molecular species in the ISM, and dust continuum emission. One of the brightest (and thus most commonly observed) FIR lines is the fine-structure transition of singly ionized carbon [C II] $158\mu\text{m}$, which traces mainly the neutral atomic gas in the ISM (Stacey et al. 1991; Hollenbach & Tielens 1999; Wolfire et al. 2003). The dust continuum is the thermal radiation emitted by dust grains heated by the UV and optical light coming from young stars (see e.g. Draine 1989; Meurer et al. 1999; Calzetti et al. 2000; Weingartner & Draine 2001; Draine 2003).

Dust grains span a wide range of physical temperatures deepening on their own physical properties and the radiation field heating them (see e.g. Draine 2003). Nevertheless, under the approximation of thermal equilibrium, the FIR spectral energy distribution (SED) can be well approximated by an isothermal grey-body function (Hildebrand 1983). Where available, observations at rest-frame Mid-Infrared (MIR) wavelengths, short-wards of the FIR emission peak, have shown significant deviations from a grey-body (Dunne & Eales 2001; Blain et al. 2003; Kovács et al. 2010; Casey 2012; Dale et al. 2012; Galametz et al. 2012; Kirkpatrick et al. 2012; da Cunha et al. 2008; da Cunha et al. 2015; Casey et al. 2018; Reuter et al. 2020). Unfortunately, MIR wavelengths are inaccessible at $z > 5$ with current instruments. Given the limited availability of observations sampling the full dust emission regime, the most common and physically-sound approach is to assume isothermal dust emitting as a grey-body. The key dust properties constrained through SED fitting are the dust temperature T_d and mass M_d^1 , which are degenerate quantities.

Reliably determining high- z galaxies T_d and M_d holds the key to many problems related to early galaxy formation and evolution. For example, it might shed light on the heating produced by obscured star formation, and on the nature and processes governing the dust formation and content in the early universe

Interestingly, in the last few years several works spanning

the redshift range $0 \leq z \leq 6$ have suggested the presence of a direct correlation between T_d and redshift (see e.g. Magdis et al. 2012a; Magnelli et al. 2013; Béthermin et al. 2015; Schreiber et al. 2018; Faisst et al. 2020; Bouwens et al. 2020; Reuter et al. 2020). Combining the few available dust temperature estimates for individual galaxies at $z > 5$ with lower- z stacking results, different works came to discrepant conclusions. While Bouwens et al. (2020) have confirmed the reported linear $T_d(z)$ increase, Faisst et al. (2020) suggested instead a flattening of the relation at higher redshift. A physical and quantitative interpretation of either trend is still lacking. Previous works suggested that warm dust temperatures at high- z might result from a more compact dust geometry in high- z galaxies (w.r.t. local galaxies), with dust being mostly located in the vicinity of young stars, and thus being more efficiently heated (Liang et al. 2019; Sommovigo et al. 2020). Other works have suggested that the increasing $T_d(z)$ trend can be qualitatively ascribed to the growing specific star formation rate at high- z (Magnelli et al. 2014; Ma et al. 2016, 2019; Shen et al. 2021), together with the lower dust content of early galaxies (see e.g. Aoyama et al. 2017; Behrens et al. 2018; Shen et al. 2021; Pallottini et al. 2022). A lower dust content would in fact result in warmer dust temperatures for a given FIR luminosity L_{FIR} .

Firmer conclusions on the T_d evolution at early times have been hindered by two factors. First, the number of galaxies at $z > 5$ for which multiple FIR continuum observations are available is very limited (Hashimoto et al. 2019; Behrens et al. 2018; Harikane et al. 2020; Bakx et al. 2020; Faisst et al. 2020). In fact, most ALMA sources, when detected in dust continuum, have only a single (or very few) data point(s) at FIR wavelengths (e.g. Knudsen et al. 2016a; Bouwens et al. 2016; Pavesi et al. 2016a; Barisic et al. 2017; Bowler et al. 2018; Pavesi et al. 2019; Hashimoto et al. 2019; Tamura et al. 2019; Béthermin et al. 2020). Hence a value for T_d is often assumed *a priori* in the fitting procedure (or associated to very large experimental uncertainties). The second limiting factor is the very large scatter of measured T_d values, ranging from $T_d \simeq 25$ K (Harikane et al. 2020) up to $T_d > 80$ K in the narrow redshift range $z = 6.2 - 8.3$ (Bakx et al. 2020).

The lack of (or poor) knowledge of T_d at high- z results in very large uncertainties on M_d as well as derived galaxy properties, such as infrared luminosity (L_{IR}) and obscured star formation rate (SFR; see e.g. Sommovigo et al. 2020). In the future, the problem can be mitigated thanks to further ALMA observations in multiple higher-frequency bands (Bands 7,8,9). In fact, for galaxies at $z \gtrsim 5$ such observations sample the SED closer to the emission peak in the FIR (see Bakx et al. 2021).

To overcome the current FIR observational limitations at $z \geq 5$, in Sommovigo et al. (2021) we developed a new method aimed at simultaneously constraining T_d and M_d with a single band measurement. The main idea is to combine the widely observed fine-structure [C II] $158\mu\text{m}$ line with the underlying dust continuum emission at the same frequency (1900 GHz).

Our method can improve the reliability of the interpretation of [C II] and continuum observations from millimetre interferometers. This is particularly relevant in the context of recent ALMA large programs targeting [C II] emitters at $z \gtrsim 5$, such as the very recent “*Reionization Era Bright Emission Line Survey*” (REBELS; PI: Bouwens, Bouwens et al. 2021). REBELS studied 40 of the brightest known galaxies

¹ An additional parameter is the dust emissivity, β_d ; see Section 2.

at $z > 6.5$ identified over a 7 deg^2 area of the sky, systematically scanning for bright ISM-cooling lines, [C II]158 μm and [O III]88 μm , and dust-continuum emission (for further details see also [Fudamoto et al. 2021](#)).

REBELS galaxies are UV-selected sources at redshift $z = 6.5 - 7.7$ ($-21.3 \lesssim M_{\text{UV}} \lesssim -22.5$); they are luminous galaxies with stellar masses² in the range $10^9 \lesssim M_*/M_\odot \lesssim 10^{10}$, and relatively high SFRs around $20 \lesssim \text{SFR}/M_\odot\text{yr}^{-1} \lesssim 200$ ([Bouwens et al. 2021](#)).

Here we apply our method ([Sommovigo et al. 2021](#)) to the 13 REBELS targets detected both in continuum (3σ) and in [C II] (5σ) at $z = 6.5 - 8.5$ (for the sources properties see [Table 1](#)). They represent the first statistical sample of continuum detections at such early epochs, featuring a four-fold increase of the size of the previously available galaxy sample.

Constraining the dust temperatures and masses of REBELS galaxies is crucial for a better understanding of SF obscuration and dust production in these early galaxies. Moreover, our analysis on the REBELS sample can investigate for the first time the reported cosmic dust temperature evolution ([Magdis et al. 2012a](#); [Magnelli et al. 2013](#); [B  thermin et al. 2015](#); [Schreiber et al. 2018](#); [Faisst et al. 2020](#); [Bouwens et al. 2020](#)) into the Epoch of Reionization. In particular, the eventual flattening in the $T_d(z)$ evolution would be more robustly identified at the high ($z \approx 7$) redshift of the REBELS sample.

This paper is organised as follows. In [Section 2](#) we summarize the [Sommovigo et al. \(2021\)](#) method to compute T_d , which is then applied to REBELS galaxies in [Section 3](#). [Section 4](#) is devoted to the analysis of the reported T_d -redshift relation in the light of the derived REBELS results. There we introduce a new physical model to explain the observed increasing T_d - z trend. In [Section 5](#) a summary and discussion of the results is given.

Throughout the paper, we assume a Λ CDM model with the following cosmological parameters: $\Omega_M = 0.3075$, $\Omega_\Lambda = 1 - \Omega_M$, $\Omega_B = 0.0486$, $h = 0.6774$, and $\sigma_8 = 0.81$. Ω_M , Ω_Λ , Ω_B are the total matter, vacuum, and baryonic densities, in units of the critical density; h is the Hubble constant in units of 100 km s^{-1} , and σ_8 is the late-time fluctuation amplitude parameter ([Planck Collaboration et al. 2016](#)).

2 METHOD

In [Sommovigo et al. \(2021\)](#) we proposed a novel method to derive the dust temperature in galaxies, based on the combination of the 1900 GHz continuum and the super-imposed

² derived from rest-frame UV SED fitting by [Stefanon & al., in prep. \(2022\)](#) using BEAGLE ([Chevallard & Charlot 2016](#)). The authors adopt a constant Star Formation History (SFH), 0.2 Z_\odot metallicity, a [Calzetti et al. \(2000\)](#) dust extinction law, and a [Chabrier \(2003\)](#) 0.1 – 300 M_\odot initial mass function. Note that the correction on the given M_* values, required to be consistent with a Salpeter 1 – 100 M_\odot IMF (used in the rest of the paper), is well within their uncertainties and does not affect significantly our results. We caution that using a non-parametric prescription for the SFH might result in M_* values up to a factor $\sim \times 3$ larger (for a detailed discussion on this point see [Topping & al., in prep. 2022](#)). Implications on the results presented here are discussed in the text.

[C II] line emission. We summarize the method in the following.

We use the [C II] luminosity, L_{CII} , as a proxy for the total gas mass M_g , or equivalently the dust mass M_d , given a dust-to-gas ratio D :

$$M_d = DM_g = D\alpha_{\text{CII}}L_{\text{CII}}, \quad (1)$$

where α_{CII} is the [C II]-to-total gas conversion factor.

We derive an analytic expression for α_{CII} using empirical relations such as the Kennicutt–Schmidt relation ([Kennicutt 1998](#), hereafter, KS), and the De Looze relation between L_{CII} –SFR ([De Looze et al. 2014](#), hereafter, DL). This yields

$$\alpha_{\text{CII}} = 32.47 \frac{y^2}{\kappa_s^{5/7}} \Sigma_{\text{SFR}}^{-0.29} \frac{M_\odot}{L_\odot}, \quad (2)$$

where Σ_{SFR} is the SFR surface density, and κ_s is the “burstiness parameter” ([Ferrara et al. 2019](#); [Pallottini et al. 2019](#); [Vallini et al. 2020](#)) which quantifies upwards deviations from the KS relation ($\kappa_s > 1$ for starbursts³). The factor $y = r_{\text{CII}}/r_* > 1$ is introduced since there is growing evidence ($1.5 \lesssim y \lesssim 3$ at $z > 4$, see e.g. [Carniani et al. 2017, 2018](#); [Matthee et al. 2017, 2019](#); [Fujimoto et al. 2019](#); [Rybak et al. 2019](#); [Fujimoto et al. 2020](#); [Ginolfi et al. 2020](#); [Carniani et al. 2020](#)) that at $z > 4$ [C II] emission (size r_{CII}) is more extended than the UV size (r_*).

We assume the dust-to-gas ratio D to scale linearly with metallicity down to $Z \lesssim 0.1 Z_\odot$ ([James et al. 2002](#); [Draine & Li 2007](#); [Galliano et al. 2008](#); [Leroy et al. 2011](#); [R  my-Ruyer et al. 2014](#)):

$$D = D_\odot \left(\frac{Z}{Z_\odot} \right), \quad (3)$$

where $D_\odot = 1/162$ is the Galactic value ([R  my-Ruyer et al. 2014](#)). This simple linear $D - Z$ relation is confirmed to hold in simulated galaxies at $z \sim 7$ for stellar masses in the range $10^9 < M_*/M_\odot < 10^{11}$ ([Dayal & al., in prep. 2022](#), see also [Ma et al. 2016](#); [Torrey et al. 2019](#)).

Armed with an expression for α_{CII} , D , and thus M_d (eq. 1), we can constrain T_d using the continuum flux at 1900 GHz. We consider Milky Way-like dust⁴, for which standard values for the dust opacity⁵ $\kappa_\nu = \kappa_*(\nu/\nu_*)^{\beta_d}$ are $(\kappa_*, \nu_*, \beta_d) = (10.41 \text{ cm}^2\text{g}^{-1}, 1900 \text{ GHz}, 2.03)$ ([Weingartner & Draine 2001](#); [Draine 2003](#)).

In [Sommovigo et al. \(2021\)](#) we rewrite the equation for the continuum flux emitted by a given dust mass⁶ with (CMB-corrected) equilibrium temperature T_d , yielding the following explicit expression for T_d :

$$T_d = \frac{T_0}{\ln(1 + f^{-1})}, \quad (4)$$

where $T_0 = h\nu_0/k_B = 91.86 \text{ K}$ is the temperature corresponding to the [C II] transition energy at $\nu_0 = 1900 \text{ GHz}$, k_B and h_P

³ $\kappa_s = 1$ for normal galaxies, being defined as $\kappa_s = \Sigma_{\text{SFR}}/(10^{-12} \Sigma_{\text{gas}}^{1.4})$ ([Heiderman et al. 2010](#))

⁴ Milky Way-like dust seems the best suited to reproduce high- z sources properties, see ([Bowler et al. 2018](#); [Schouws et al. 2021](#); [Ferrara & al., in prep. 2022](#)) for a detailed discussion.

⁵ This power-law approximation for the dust opacity is valid at wavelengths $\lambda > 20 \mu\text{m}$, well within the FIR range.

⁶ assuming an isothermal, optically-thin dust emission model

Table 1. On the left: Measured REBELS galaxies properties, respectively: redshift z , stellar mass $\log M_\star$, [C II] luminosity L_{CII} , and 1900 GHz continuum flux F_{1900} (not CMB-corrected). For the data analysis we refer to the dedicated papers by [Inami & al., in prep. 2022](#) (F_{1900}), [Schouws & al., in prep. 2022](#) (z, L_{CII} , see also [Bouwens et al. 2021](#)), and [Stefanon & al., in prep. 2022](#) (M_\star). On the right: Predicted REBELS galaxies properties, respectively: [C II]-to-total gas conversion factor α_{CII} (eq. 2), dust temperature T_d and mass M_d , IR luminosity $\log L_{\text{IR}}$, SN dust yield y_d and obscured SFR, $\text{SFR}_{\text{IR}}[M_\odot\text{yr}^{-1}] = 10^{-10} L_{\text{IR}}[L_\odot]$ ([Kennicutt 1998](#)). Please note that the galaxy names in the text are abbreviated as REBxx for conciseness.

Measured				ID#	Predicted					
z	$\log M_\star$	L_{CII}	F_{1900}		α_{CII}	T_d	$\log M_d$	$\log L_{\text{IR}}$	y_d	SFR_{IR}
	$[M_\odot]$	$[10^8 L_\odot]$	$[\mu\text{Jy}]$			$[\text{K}]$	$[M_\odot]$	$[L_\odot]$	$[M_\odot]$	$[M_\odot\text{yr}^{-1}]$
6.496	$9.2^{+0.9}_{-1.0}$	6.9 ± 0.4	67 ± 13	REB05	5^{+4}_{-2}	43^{+15}_{-9}	$7.14^{+0.31}_{-0.3}$	$11.37^{+0.5}_{-0.32}$	$0.51^{+0.52}_{-0.26}$	23^{+51}_{-12}
6.749	$9.0^{+0.6}_{-0.7}$	7.4 ± 0.9	101 ± 20	REB08	5^{+3}_{-2}	50^{+17}_{-11}	$7.17^{+0.25}_{-0.25}$	$11.83^{+0.5}_{-0.36}$	$0.74^{+0.58}_{-0.33}$	68^{+147}_{-39}
7.346	$8.9^{+0.9}_{-0.7}$	10.1 ± 1.9	87 ± 24	REB12	4^{+2}_{-1}	49^{+16}_{-9}	$7.19^{+0.22}_{-0.22}$	$11.79^{+0.49}_{-0.41}$	$0.93^{+0.6}_{-0.33}$	62^{+130}_{-33}
7.084	$8.7^{+0.8}_{-0.7}$	3.7 ± 0.5	60 ± 15	REB14	6^{+3}_{-1}	52^{+15}_{-10}	$6.95^{+0.25}_{-0.23}$	$11.67^{+0.44}_{-0.34}$	$0.87^{+0.59}_{-0.36}$	47^{+84}_{-25}
7.675	$9.5^{+0.6}_{-0.7}$	10.8 ± 0.7	53 ± 10	REB18	4^{+5}_{-2}	39^{+12}_{-7}	$7.30^{+0.34}_{-0.32}$	$11.29^{+0.4}_{-0.21}$	$0.34^{+0.4}_{-0.18}$	19^{+30}_{-7}
7.370	$8.8^{+0.7}_{-0.7}$	8.7 ± 1.7	71 ± 20	REB19	3^{+2}_{-1}	50^{+16}_{-9}	$7.09^{+0.19}_{-0.24}$	$11.74^{+0.48}_{-0.32}$	$1.05^{+0.57}_{-0.45}$	55^{+110}_{-28}
7.307	$9.9^{+0.2}_{-0.2}$	15.9 ± 0.4	260 ± 22	REB25	5^{+3}_{-1}	55^{+15}_{-14}	$7.55^{+0.34}_{-0.22}$	$12.45^{+0.43}_{-0.45}$	$0.24^{+0.37}_{-0.1}$	284^{+480}_{-184}
7.090	$9.7^{+0.3}_{-0.3}$	6.1 ± 0.6	51 ± 10	REB27	5^{+7}_{-2}	41^{+15}_{-9}	$7.14^{+0.37}_{-0.32}$	$11.25^{+0.48}_{-0.3}$	$0.15^{+0.2}_{-0.08}$	18^{+37}_{-9}
6.685	$9.6^{+0.2}_{-0.4}$	5.5 ± 0.9	56 ± 13	REB29	6^{+7}_{-1}	42^{+16}_{-10}	$7.11^{+0.37}_{-0.32}$	$11.27^{+0.53}_{-0.35}$	$0.16^{+0.22}_{-0.09}$	19^{+44}_{-10}
6.729	$9.6^{+0.4}_{-0.4}$	7.9 ± 0.6	60 ± 17	REB32	5^{+6}_{-2}	39^{+15}_{-9}	$7.21^{+0.35}_{-0.32}$	$11.22^{+0.51}_{-0.31}$	$0.24^{+0.31}_{-0.13}$	17^{+37}_{-9}
6.577	$9.6^{+0.7}_{-1.3}$	16.8 ± 1.3	163 ± 23	REB38	4^{+4}_{-1}	46^{+18}_{-11}	$7.45^{+0.32}_{-0.3}$	$11.89^{+0.55}_{-0.38}$	$0.39^{+0.43}_{-0.2}$	77^{+195}_{-45}
6.845	$8.6^{+0.6}_{-0.6}$	7.9 ± 1.4	80 ± 16	REB39	3^{+1}_{-1}	58^{+15}_{-9}	$6.95^{+0.13}_{-0.19}$	$11.98^{+0.4}_{-0.29}$	$1.3^{+0.46}_{-0.45}$	95^{+145}_{-46}
7.365	$9.5^{+0.5}_{-1.0}$	4.9 ± 1.0	48 ± 13	REB40	6^{+7}_{-3}	43^{+17}_{-10}	$7.07^{+0.37}_{-0.32}$	$11.34^{+0.54}_{-0.34}$	$0.21^{+0.27}_{-0.11}$	22^{+54}_{-12}

are the Boltzmann and Planck constants, respectively. The function f is defined as:

$$f = \mathcal{B}(T_{\text{CMB}}) + A^{-1} \tilde{F}_{\nu_0}, \quad (5)$$

where $\mathcal{B}(T_{\text{CMB}}) = [\exp(T_0/T_{\text{CMB}}) - 1]^{-1}$, and T_{CMB} is the CMB temperature at a given redshift. The non-dimensional continuum flux \tilde{F}_{ν_0} and the constant⁷ A correspond to:

$$\tilde{F}_{\nu_0} = 0.98 \times 10^{-16} \left(\frac{F_{\nu_0}}{\text{mJy}} \right), \quad (6)$$

$$A = 4.33 \times 10^{-24} \left[\frac{g(z)}{g(6)} \right] \left(\frac{L_{\text{CII}}}{L_\odot} \right) \left(\frac{\alpha_{\text{CII}}}{M_\odot/L_\odot} \right) D,$$

where $g(z) = (1+z)/d_L^2$, and d_L is the luminosity distance to redshift z . Eq. 4 can be used to compute T_d using a single 1900 GHz observation (which provides both L_{CII} and F_{ν_0}) modulo an estimate for D (eq. 3) and α_{CII} (eq. 2).

Writing explicitly the expressions for D and α_{CII} it turns out that T_d is ultimately a function of $(\kappa_s, z, F_{\nu_0}, Z, \Sigma_{\text{SFR}}, L_{\text{CII}}, y)$. All these parameters are generally constrained by observations out to very high redshift with two exceptions. Both κ_s and the metallicity Z are largely unknown. Hence in the derivation we consider a broad random uniform distribution for both parameters (see Section 3). To optimally constrain T_d , we add the following broad physical conditions:

□ M_d cannot exceed the maximal dust production per supernova (SN), $M_{d,\text{max}} = 0.04 M_\star^8$. This expression for $M_{d,\text{max}}$ is obtained by assuming a standard Salpeter 1 – 100 M_\odot Initial Mass Function (IMF, [Ferrara & Tolstoy 2000](#)), and that all the SN metal yield ($\approx 2 M_\odot$ per SN) gets locked into dust grains (see eq. 15 in [Sommovigo et al. 2021](#)).

⁷ Note that the value given here is 20% lower w.r.t. the one given in [Sommovigo et al. \(2021\)](#) due to the slightly different dust model

⁸ Note that to set this broad upper limit we do not account for dust destruction.

□ The IR-deduced star formation, $\text{SFR}_{\text{IR}} = 10^{-10} L_{\text{IR}}$ ([Kennicutt 1998](#)), cannot largely exceed the SFR deduced from [C II] using the DL relation for starbursts⁹.

We recall that the relation

$$L_{\text{IR}} = \left(\frac{M_d}{M_\odot} \right) \left(\frac{T_d}{8.5 \text{ K}} \right)^{4+\beta_d} L_\odot. \quad (7)$$

holds for the dust model adopted here ([Ferrara & al., in prep. 2022](#)). Solutions not satisfying both these two bounds are discarded. These conditions result in a lower (upper) cut on T_d corresponding to unphysically large dust masses (FIR luminosities/SFR). This allows us to effectively constrain T_d at high- z despite of the lack of information on (κ_s, Z) .

This method for the dust temperature derivation has been tested on a sample of 19 local galaxies and four galaxies at $z \gtrsim 4$ ([Sommovigo et al. 2021](#); [Bakx et al. 2021](#)). For all these galaxies multiple data points in the FIR SED are available, allowing us to compare our inferred dust temperatures with robust T_d estimates obtained with traditional SED fitting. For the 19 local galaxies all the parameters $(\kappa_s, z, F_{\nu_0}, Z, \Sigma_{\text{SFR}}, L_{\text{CII}}, y)$ are constrained by observations. This is also true for 3 out of the 4 high- z galaxies considered in the test¹⁰. For the remaining high- z galaxy, A1689-zD1 at $z = 7.13$, both (κ_s, Z) are unknown hence we assume the same broad distributions of values considered here for REBELS galaxies ($Z = 0.3 - 1 Z_\odot$ and $\kappa_s = 1 - 50$). These assumptions are motivated in detail in

⁹ Precisely, we allow SFR_{IR} to deviate at most by $\lesssim 1$ dex from $\text{SFR}/(M_\odot\text{yr}^{-1}) = 10^{-7.06} L_{\text{CII}}/L_\odot$ ([De Looze et al. 2014](#)), which is comparable to the dispersion around this relation observed at high- z (see e.g. [Carniani et al. 2020](#))

¹⁰ For reference, in the considered local galaxies: $0.05 \lesssim Z/Z_\odot \lesssim 2.75$, $0.1 \lesssim \kappa_s \lesssim 5.9$ and [C II] emitting regions are as extended as stars ($y \sim 1$). For the 3 high- z galaxies SPT0418-47, MACS416-Y1 and B14-65666: $0.2 \lesssim Z/Z_\odot \lesssim 0.4$, $9 \lesssim \kappa_s \lesssim 45$ and $1.2 \lesssim y \lesssim 1.5$.

Sec. 3. Encouragingly, we recovered consistent dust temperatures with traditional SED fitting within 1σ spanning the very large redshift range $z = 0 - 8.31$ (as well as the large temperature range $20 \text{ K} \lesssim T_d \lesssim 100 \text{ K}$).

We also tested our method on simulations, applying it to the $z \sim 6.7$ galaxy Zinnia (a.k.a. serra05:s46:h0643) from the SERRA simulation suite (Pallottini et al. 2019, see also Pallottini et al. 2022). Also in this case, we recover T_d in agreement with single-temperature grey body SED fitting performed at the frequencies corresponding to ALMA bands 6, 7, and 8.

In (Sommovigo et al. 2021) we have shown that the dust temperature derived from our method matches that obtained from FIR SED fitting. We underline that this single value, which we refer to as T_d throughout the paper, does not necessarily correspond to the dust physical temperature, which is instead characterised by a Probability Distribution Function (PDF, see e.g. Behrens et al. 2018; Sommovigo et al. 2020).

In general, T_d does not necessarily provide a statistically sound representation of the PDF. We investigated the relation between the two in Appendix A of Sommovigo et al. (2021) for the simulated galaxy Zinnia. At $z \gtrsim 5$ such detailed comparison with observations is not currently possible due to the lack of information on the galaxies dust temperature PDF. In the case of Zinnia, we found that T_d corresponds to the galaxy mass-weighted dust temperature ($\sim 60 \text{ K}$), which is a factor $\sim 2\times$ colder than the luminosity-weighted dust temperature. In fact, Zinnia shows an excess of emission at MIR wavelengths (which is not traced by T_d) due to the presence of a scarce, but very luminous, hot dust component. The generalization of such PDF- T_d relation is pending on a thorough comparison with a larger number of simulated galaxies, and future instruments observations possibly providing MIR-to-IR coverage for $z \gtrsim 5$ galaxies (such as the yet to be launched space telescopes Millimetron, see e.g. Novikov et al. 2021, and Origins, see e.g. Wiedner et al. 2021).

Finally, we remark that the increase by a factor ~ 3 in the stellar masses, which might result from using a non parametric SFH (Topping & al., in prep. 2022), barely affects our results. In fact, the derived values of α_{CII} , M_d , and T_d of individual galaxies remain nearly unaffected, given their uncertainties, even by varying the stellar-mass based upper limits on M_d by that amount.

3 APPLICATION TO REBELS GALAXIES

We use our method to derive T_d for the 13 REBELS galaxies that are detected both in [C II] and in the continuum at 1900 GHz. In this work we always refer to this sub-sample of the survey targets. The observed properties of these sources are summarized in Table 1. For the data analysis we refer to the dedicated papers by Inami & al., in prep. 2022 (FIR continuum fluxes), Schouws & al., in prep. 2022 ([C II] luminosities), and Stefanon & al., in prep. 2022 (stellar masses).

For some of the REBELS sources the UV half-light radius has been measured by Bowler et al. (2017), who find on average $r_\star = 1.3 \pm 0.8 \text{ kpc}$. Bowler et al. (2017) caution that the large sizes $r_\star > 1 \text{ kpc}$ are due to multiple components, with individual clumps being less extended $r_\star \sim 0.2 - 1.0 \text{ kpc}$. This is in agreement with the theoretical findings by Ferrara & al., in prep. (2022), who predicts sub-kpc sizes for most REBELS

galaxies. In light of this, we consider star-forming/dust emitting regions of REBELS galaxies to be uniformly randomly distributed in the range $0.2 \text{ kpc} \lesssim r_\star \lesssim 1.1 \text{ kpc}$.

We then consider the [C II] emitting regions to be $1.5 \lesssim y \lesssim 3$ times more extended than the UV emitting ones, as indicated by previous observations of galaxies at $z \gtrsim 4$ (see e.g. Carniani et al. 2017, 2018; Matthee et al. 2017, 2019; Fujimoto et al. 2019, 2020; Ginolfi et al. 2020; Carniani et al. 2020).

The burstiness parameter of REBELS galaxies is unknown. High- z UV selected sources are expected to be highly star forming and UV emitting by construction (Dayal et al. 2013). Both locally and at intermediate redshift, values up to $\kappa_s \approx 100$ have been observed in such galaxies (see e.g. Daddi et al. 2010). Recently, Vallini et al. (2020) found for the mildly star-bursting COS-3018 at $z = 6.854$ a value of $\kappa_s \sim 3$, applying the [C II]-emission model given in Ferrara et al. (2019). Applying the same method on 11 bright UV selected galaxies¹¹ at $z = 6 - 9$, Vallini et al. (2021) find values as large as $10 \lesssim \kappa_s \lesssim 80$. For the REBELS galaxies we choose a random uniform distribution in the range $1 \lesssim \kappa_s \lesssim 50$ inline with the independent derivation in Ferrara & al., in prep. (2022) which suggests that these sources are not extreme starbursts.

For the metallicity, which is also unconstrained by current data, we assume a broad uniform random distribution in the range $0.3 - 1 Z_\odot$. This general assumption is validated by numerical simulations of galaxies at $z \sim 6$ with similar stellar masses $10^9 < M_\star < 10^{11}$ (Ma et al. 2016; Torrey et al. 2019), and several observational studies which analyse FIR lines (such as [N II], [N III], [C II], and [O III]) at $z \gtrsim 6 - 8$ to derive Z (see e.g. Pereira-Santaella et al. 2017; Hashimoto et al. 2019; De Breuck et al. 2019; Tamura et al. 2019; Vallini et al. 2020; Bakx et al. 2020; Jones et al. 2020, and references therein). Current estimates of Z at high redshift will be significantly ameliorated thanks to forthcoming ALMA observations and to the James Web Space Telescope (JWST) spectroscopy¹².

We pause for a quick summary: the physical properties needed for the application of our method are $(\kappa_s, z, F_{\nu_0}, Z, \Sigma_{\text{SFR}}, L_{\text{CII}}, y)$. For REBELS galaxies all these properties are constrained by observations, with the exception of (y, κ_s, Z) . For these three parameters, for each individual REBELS galaxy, we assume uniform random distributions in the broad ranges $1.5 \lesssim y \lesssim 3$, $1 \lesssim \kappa_s \lesssim 50$, and $0.3 < Z/Z_\odot < 1$, as motivated in the previous paragraphs.

Using eq. 2 we compute the [C II]-to-total gas conversion coefficient α_{CII} for all REBELS galaxies. Individual values are given in Table 1, the average is $\langle \alpha_{\text{CII}} \rangle = 5.3^{+0.8}_{-1.2}$. We note that this value is lower than the values we find in local galaxies (Sommovigo et al. 2021, $10 \lesssim \alpha_{\text{CII}} \lesssim 10^3$ at $z \sim 0$). Interestingly, we find low $\alpha_{\text{CII}} < 7$ also in the other $z > 4$ sources analysed in Sommovigo et al. 2021 (SPT0418-47 at $z = 4.225$, B14-65666 at $z = 7.15$, and MACS0416-Y1 at $z = 8.31$). This

¹¹ In particular: MACS1149-JD1 (Hashimoto et al. 2018), A2744-YD4 (Laporte et al. 2017), MACS416-Y1 (Tamura et al. 2019; Bakx et al. 2020), SXDF-NB1006-2 (Inoue et al. 2016), B14-65666 (Hashimoto et al. 2019), BDF3299 (Carniani et al. 2017), J0121 J0235, J1211 (Harikane et al. 2020). See also Table B1, Fig. 3.

¹² JWST will provide observations of optical nebular lines (such as H β , H α , [N II], [O II] and [O III]), which are reliable metallicity tracers, out to $z \sim 10$ (see e.g. Wright et al. 2010; Maiolino & Mannucci 2019; Chevillard et al. 2019)

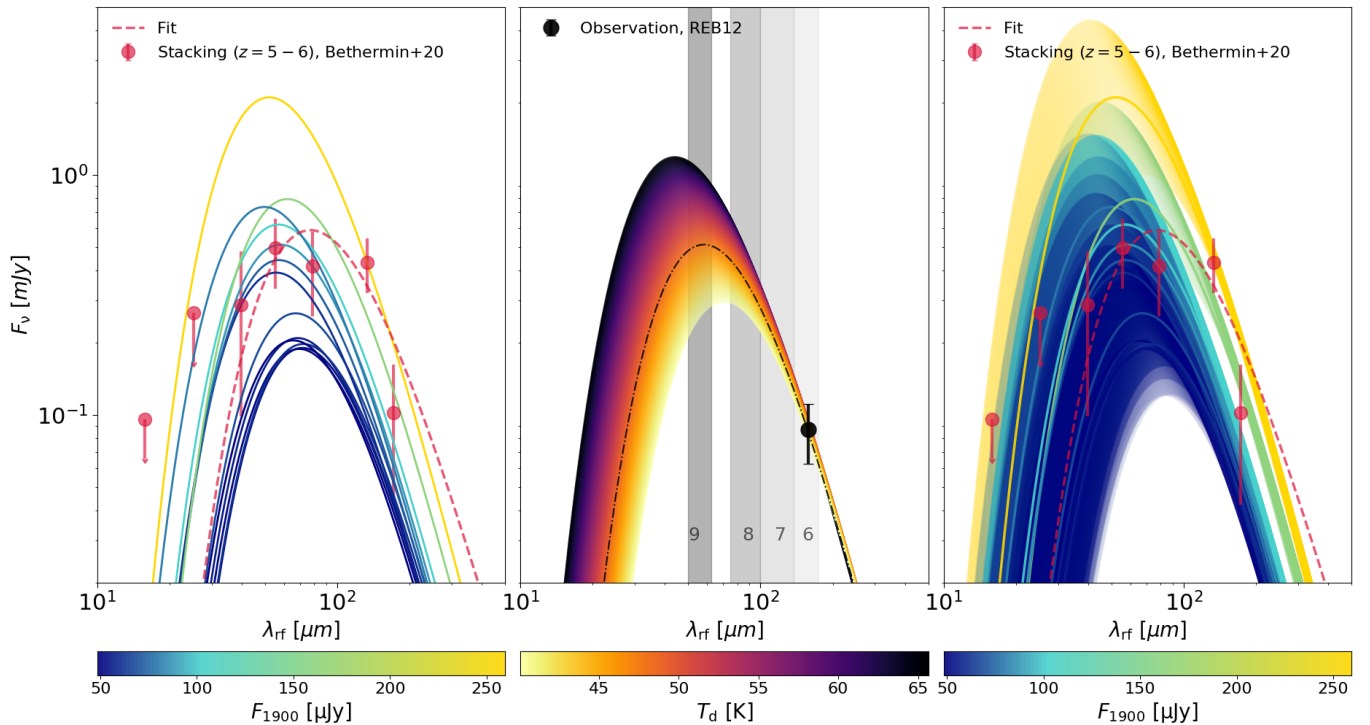


Figure 1. **Left panel:** FIR SEDs obtained using the median (T_d, M_d) derived for REBELS galaxies (see Table 1 for the sources details). The lines are colour-coded depending on their 1900 GHz flux (see colorbar). The red points are obtained by (Bethermin et al. 2020) for the ALPINE galaxies in the redshift interval $z = 5 - 6$ through stacking. The red dashed line is the best fit to these points (corresponding to $T_d \sim 42$ K); **Center:** Variation in the SED of a single source (REBELS-12) due to the $1-\sigma$ uncertainty in (T_d, M_d) around the median values. The lines are colour coded according to the corresponding dust temperature (see colorbar). The dashed black curve shows the SED for the median $T_d \sim 46$ K. The black point is the continuum observation at 1900 GHz. The shaded grey regions mark the ALMA bands 6 to 9; **Right:** Variation of the SEDs of all the REBELS galaxies due to the uncertainty in (T_d, M_d) of each source. This plot can be interpreted as the combination of the left and central panels. Here we are showing the median FIR SEDs and their variation due to uncertainty on (M_d, T_d) for all the REBELS galaxies. The colour coding, the red points and red dashed line are the same as in the left panel.

might indicate that at fixed [C II] luminosity high- z galaxies have a lower gas content (for a detailed discussion see e.g. Ferrara et al. 2019).

We conclude with a remark. The *total* gas-to-[C II] conversion factor computed here $\alpha_{\text{CII}} = \Sigma_{\text{gas}}/\Sigma_{\text{CII}}$ is different by construction from the empirical *molecular*-to-[C II] conversion factor $\alpha_{\text{CII,mol}} = \Sigma_{\text{H}_2}/\Sigma_{\text{CII}} = 31^{+31}_{-16}$ derived¹³ in Zanella et al. (2018). The ratio of the two conversion factors corresponds to $\alpha_{\text{CII,mol}}/\alpha_{\text{CII}} = f_{\text{H}_2} (r_{\text{gas}}/r_{\text{H}_2})^2 \approx f_{\text{H}_2} y^2$ (under the reasonable assumption that $r_{\text{CII}} \sim r_{\text{gas}}$ and $r_{\text{H}_2} \sim r_*$), where $f_{\text{H}_2} = M_{\text{H}_2}/M_{\text{gas}}$ is the molecular gas fraction. Since $f_{\text{H}_2} < 1$ by definition, the empirical result $\alpha_{\text{CII,mol}} \sim 31$ can be reconciled with the REBELS galaxies average value of $\langle \alpha_{\text{CII}} \rangle = 5.3$ for $y > 2.4$.

We proceed to compute M_d and T_d for all our targets. The results are summarised in Table 1, and discussed in detailed in the following dedicated Sections.

3.1 Dust temperatures

We find the median T_d of REBELS galaxies to vary in the range between 39 K and 58 K with REBELS-39 (REBELS-18,32) being the galaxy with the warmest (coldest) dust. The median values are associated with large uncertainties (up to $\sim 35\%$) due to the lack of knowledge on the metallicity and burstiness of REBELS galaxies. Considering such uncertainties, the range widens to 30 K – 73 K (where the lower limit is set by the condition on the dust masses and the upper one by that on the obscured SFRs, see Section 2). Note that these large uncertainties on T_d are often comparable with the ones derived in the literature from traditional SED fitting using 2 – 3 data points at FIR wavelengths (see Table B1 where we compare T_d values obtained from our method vs. SED fitting for several $z > 5$ galaxies). Further ALMA observations in bands 8 – 9 will help us significantly in constraining T_d at high- z by sampling the SEDs closer to the FIR emission peak (see central panel of Fig. 1).

Overall we find an average dust temperature of $\langle T_d \rangle = 47 \pm 6$ K. This value is in agreement with the independent derivation in Ferrara & al., in prep. (2022), where they find $\langle T_d \rangle = (52 \pm 12)$ K. The physical model presented in Ferrara & al., in prep. (2022) relies on 1900 GHz continuum, and UV data (instead of [C II] used here) to derive the physical properties of individual REBELS galaxies, such as

¹³ In Sommovigo et al. (2021) we derive an analytical formula also for $\alpha_{\text{CII,mol}} \approx 30.3 t_{\text{depl,H}_2}/\text{Gyr}$, finding consistent values with Zanella et al. (2018) under the assumption of a molecular gas depletion time $t_{\text{depl,H}_2} = 0.4 - 0.7$ Gyr (Walter et al. 2020).

their ($T_d, M_d, L_{\text{IR}}, \text{SFR}$), assuming assuming a given attenuation curve.

The average value (T_d) $\simeq 47$ K is close to the dust temperature derived by [Bethérmin et al. \(2020\)](#) from the mean stacked SED of ALPINE sources (and analogs in the COSMOS field) in the redshift interval $z = 5 - 6$ ($T_d = 43 \pm 5$ K). For the lower redshift bin at $z = 4 - 5$, where they have $3\times$ more sources (analogs included), [Bethérmin et al. \(2020\)](#) produce two different mean stacked SEDs dividing the considered sources depending on their SFR. For the galaxies with lower SFR (SFR $> 10 M_\odot/\text{yr}$) they find $T_d = 41 \pm 1$ K, while for the higher star forming galaxies (SFR $> 100 M_\odot/\text{yr}$) they find $T_d = 47 \pm 2$ K.

Since most REBELS galaxies have SFR $\lesssim 100 M_\odot/\text{yr}$ (both from the DL relation, and from the independent analysis of rest-frame UV and IR data performed in [Ferrara & al., in prep. 2022](#)), they overall appear to have similar dust temperatures to the lower redshift ALPINE galaxies. We discuss this point in detail in the dedicated Section 4.

3.2 Dust masses

We find the median dust masses of REBELS sources to vary in the range $6.95 \leq \log(M_d/M_\odot) \leq 7.55$, REBELS-25 (REBELS-14,39) being the galaxy with the largest (lowest) dust mass. This is not surprising as REBELS-25 also has the largest stellar mass $M_\star \sim 10^{10} M_\odot$ and continuum emission $F_{1900} = 260 \pm 22 \mu\text{Jy}$ in the sample. Overall we find an average dust mass around $\langle M_d \rangle = (1.63 \pm 0.73) \times 10^7 M_\odot$. This value is consistent with an independent derivation in [Ferrara & al., in prep. \(2022\)](#) ($\langle M_d \rangle = (1.3 \pm 1.1) \times 10^7 M_\odot$), although they find a larger scatter in the dust masses values.

We also compute the dust yield per SN, y_d , required to produce REBELS galaxies dust masses. We use that: $y_d = M_d/M_\star \nu_{\text{SN}}$, where $\nu_{\text{SN}} = (53 M_\odot)^{-1}$ is the number of SNe per solar mass of stars formed ([Ferrara & Tolstoy 2000](#)) assuming a Salpeter 1 – 100 M_\odot IMF. For all (but two of) the REBELS sources we find $y_d \lesssim 1 M_\odot$ (see Table 1 for the value of y_d in each galaxy), which is quite consistent with the latest constraints on SNe dust production by [Leńniewska & Michałowski \(2019\)](#). They find that up to $y_d = 1.1 M_\odot$ of dust per SN can be produced, where the exact value depends on the amount of dust which is destroyed/ejected during the SN explosion (1.1 M_\odot corresponds to the case of no dust destruction/ejection).

We note that SN yield is still highly debated, with some works suggesting that dust destruction processes might only spare $\lesssim 0.1 M_\odot$ per SN (e.g., [Bocchio et al. 2016](#); [Matsuura et al. 2019](#); [Slavin et al. 2020](#)). In this extreme case, interstellar medium grain growth or more exotic dust production mechanisms might be required ([Mancini et al. 2015](#); [Michałowski 2015](#); [Graziani et al. 2020](#)).

It is worth mentioning that the increase by a factor ~ 3 of the stellar masses possibly resulting from a non parametric SFH prescription would have a relevant impact in this context. In fact, as explained in Sec. 2, the dust masses remain mostly unaffected. This implies, by definition, a reduction by the same factor ~ 3 in the SN dust yield. As a result, we would find an average value of $\langle y_d \rangle \sim 0.23 M_\odot$ for the REBELS sources, consistent even with stringent SN dust production constraints.

For a detailed discussion we refer to [Dayal & al., in prep.](#)

(2022) where they use the semi-analytical galaxy formation model DELPHI to investigate the dust build up and content of average $z \sim 7$ galaxies. The processes accounted for include SNe dust production, grain growth, astration, shock destruction, and ejection in outflows. The DELPHI model general predictions are then compared to the dust masses derived here for individual REBELS galaxies, finding a good agreement in most (77%) cases.

3.3 IR emission

In Fig. 1 we show the FIR SEDs obtained for the REBELS galaxies considering a single-temperature grey body approximation and the dust masses and temperatures in Table 1. In the left panel we show the FIR SEDs obtained using the median (T_d, M_d) values of each source. We can see that the flux at the peak of emission changes within a factor $\times 10$, with a variation in the peak wavelength of emission $50 \mu\text{m} \leq \lambda_{\text{peak}} \leq 73 \mu\text{m}$. Interestingly, almost all the λ_{peak} values that we predict lay within the range observable with ALMA, albeit in band-10 for the hottest sources.

For the FIR SED of each source we refer to Appendix A. Here we focus on REBELS-12 (central panel of Fig. 1), whose M_d and T_d are close to the average values in the sample. For REBELS-12 cold dust temperatures $T_d < 30$ K are disfavoured as they would result in very large dust masses $M_d \gg 10^7 M_\odot$, and very low κ_ν values that are unexpected for a strongly UV-emitting high- z source. Very hot dust temperatures ($T_d > 80$ K) are similarly unlikely as they would result in very large IR luminosities, and consequently unreasonably large obscured SFRs (for REBELS-12 SFR_{IR} $> 500 M_\odot/\text{yr}$). These are hard to reconcile with the generally blue UV slopes β observed in most REBELS galaxies (e.g. $\beta = -1.99$ for REBELS-12). We briefly discuss a possible caveat in Section 5.

3.3.1 F_{1900} to total IR luminosity conversion at $z \sim 7$

Using eq. 7 we can compute the IR luminosities of all the REBELS galaxies. We find that their IR luminosities vary in the range $1.7 \times 10^{11} L_\odot \lesssim L_{\text{IR}} \lesssim 2.8 \times 10^{12} L_\odot$, which corresponds to obscured SFRs in the range $\sim 17 - 285 M_\odot/\text{yr}$ (assuming the conversion factor given in Table 1). Interestingly, the most IR luminous REBELS (REBELS-25) classifies as an Ultra-Luminous InfraRed Galaxy (ULIRG, with $L_{\text{IR}} > 10^{12} L_\odot$, see e.g. [Lonsdale et al. 2006](#)) despite being UV selected. This peculiar source will be discussed in detail in [Hygate & al., in prep. \(2022\)](#).

Combining these values with the total star formation rates derived using the DL relation for starbursts we find that on average $\langle \text{SFR}_{\text{IR}}/\text{SFR} \rangle = 53\%$ (in agreement with the independent derivation in [Schouws et al. 2021](#); [Ferrara & al., in prep. 2022](#); [Dayal & al., in prep. 2022](#)), implying that REBELS galaxies are on average relatively UV-transparent sources. The only exceptions are represented by REBELS-8, REBELS-14, REBELS-25 and REBELS-39 for which we find $\text{SFR}_{\text{IR}} \gtrsim \text{SFR}$, i.e. the SFR deduced from [C II] is exceeded (barely, only by 6%, in the case of REBELS-8). Interestingly these sources include 2 (REBELS-8, and the peculiar REBELS-25) of the 4 galaxies for which the UV-to-IR emission model in [Ferrara & al., in prep. \(2022\)](#) fails to find a solution for (T_d, M_d) (using the same dust model adopted here,

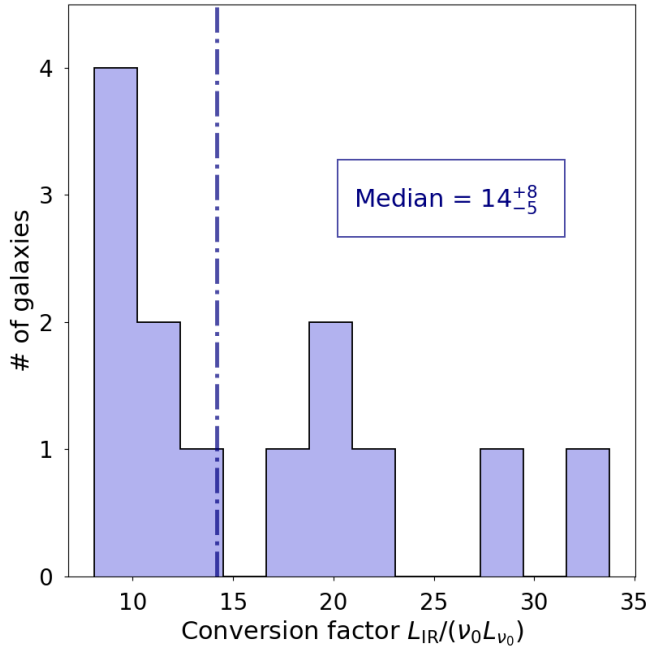


Figure 2. Conversion factor from the monochromatic luminosity $\nu_0 L_{\nu_0}$ at 1900 GHz to the total IR luminosity L_{IR} for the REBELS galaxies. We also show the median (blue line) value.

i.e. MW-like dust). In fact these galaxies have very large IR-to-UV flux ratios compared to their UV slopes. This might indicate that their UV and IR emitting regions are spatially segregated (see Ferrara & al., in prep. 2022 for a detailed discussion).

We can provide a conversion factor from the galaxies monochromatic luminosity νL_ν at any frequency to their total L_{IR} (for a discussion on the application of such conversion factor see e.g. Fudamoto et al. 2020; Bouwens et al. 2020). The monochromatic luminosity at 1900 GHz can be written as:

$$\nu_0 L_{\nu_0} = 2.92 \times 10^{11} \left[\frac{g(6)}{g(z)} \right] \left(\frac{F_{\nu_0}}{\text{mJy}} \right) L_\odot \quad (8)$$

where $g(z)$ is defined in eq. 6. The results for the conversion factor $L_{\text{IR}}/\nu_0 L_{\nu_0}$ are shown in Fig. 2.

We find a median value of $L_{\text{IR}}/\nu_0 L_{\nu_0} = 14^{+8}_{-5}$ (where both $L_{\text{IR}}, \nu_0 L_{\nu_0}$ are in solar luminosity units). This range is consistent with the one obtained in Bouwens et al. (2020) at $z \sim 7$ using a simple modified black body with $\beta_d = 1.6$, and a dust temperature derived from a linear fit of currently available dust temperature data vs. redshift. It is worth noting that they consider $T_d = 54$ K at $z = 7$, which is warmer than the temperatures derived here for the REBELS galaxies. We will discuss this point in detail in the following Section 4.

4 DUST TEMPERATURE EVOLUTION

In the last few years, several works have suggested the presence of a trend of increasing dust temperature with redshift in star forming galaxies detected in the UV-to-IR rest-frame wavelength range (Magdis et al. 2012b; Magnelli et al. 2013, 2014; Béthermin et al. 2015; Schreiber et al. 2018).

In particular, Schreiber et al. (2018) fitted stacked SEDs to a complete sample of main sequence galaxies in the CANDELS fields, and derived the linear relation $T_d = 32.9 + 4.6(z - 2)$, shown in the inset of Fig. 3. Compared to those for individual sources, stacked SEDs (a) reduce the scatter introduced in the relation by different intrinsic galaxy properties, and (b) allow to extend the relation up to $z \sim 4$. The above trend is also consistent with the stacked SED fitting results produced for ALPINE galaxies by Béthermin et al. (2020) at $4 < z < 6$ (also shown in the inset). In this case, a stacking procedure was necessary since ALPINE galaxies are individually detected only in a single band at restframe 1900 GHz. Hence it would be impossible to constrain their T_d with ordinary SED-fitting.

More recently, T_d obtained from stacked SEDs at $z < 6$ has been combined with the T_d derived for individual galaxies detected in multiple bands at $z \gtrsim 5$. Two studies reached somewhat discordant conclusions. While Liang et al. (2019); Faisst et al. (2020) deduce a flattening of $T_d - z$ relation at $z > 4$, Bouwens et al. (2020) confirm the trend with little modification in the slope.

Either trends are yet to be explained by a physical model. Previous theoretical works suggested that warmer dust temperatures at high- z might depend on the dust geometry, with most of the dust in high- z galaxies being located in compact, young star-forming regions, where the dust heating is particularly efficient (Behrens et al. 2018; Liang et al. 2019; Sommovigo et al. 2020). Other works (Magnelli et al. 2014; Ma et al. 2016, 2019; Shen et al. 2021) have suggested that the increasing $T_d(z)$ trend together with the flattening at $z \sim 4$ are correlated to the specific star formation rate increase with redshift and its subsequent plateau at $z \sim 4$ (see e.g. Tomczak et al. 2016; Santini et al. 2017). Finally the lower dust-to-metal ratio predicted for early galaxies from simulations at $z \gtrsim 5$ (see e.g. Aoyama et al. 2017; Behrens et al. 2018; Shen et al. 2021; Pallottini et al. 2022) could also motivate the presence of hot dust at high- z . In fact, a lower dust content results in warmer dust temperatures for a given L_{FIR} .

Our analysis of the REBELS sample can clarify the issue of the $T_d(z)$ evolution in a unique way for two reasons: (a) REBELS continuum detections double the number of previously known sources at $z \gtrsim 5$; (b) possible deviations from the linear trend are more robustly identified at the higher ($z \approx 7$) redshift of the REBELS sample.

Extrapolating the Schreiber et al. (2018) relation to $z = 7$ gives $T_d = (56 \pm 4)$ K, i.e. a slightly warmer temperature than found here, $T_d \sim 47$ K. This does not come as a surprise, as there is no special physical motivation to expect a linearly increasing T_d trend. It is therefore crucial to develop a simple but physical theoretical framework against which observations of individual UV-to-FIR detected galaxies in the range $0 \lesssim z \lesssim 8.5$ can be compared and interpreted. This is our goal in the next Section.

4.1 Physical origin of the $T_d - z$ relation

Under the assumption that FIR and UV emitting regions are co-spatial, L_{IR} is equal to the absorbed fraction of the intrinsic UV luminosity, L_{1500} :

$$L_{\text{IR}} = (1 - e^{-\tau_{\text{eff}}})L_{1500} = (1 - e^{-\tau_{\text{eff}}})\mathcal{K}_{1500}\text{SFR}. \quad (9)$$

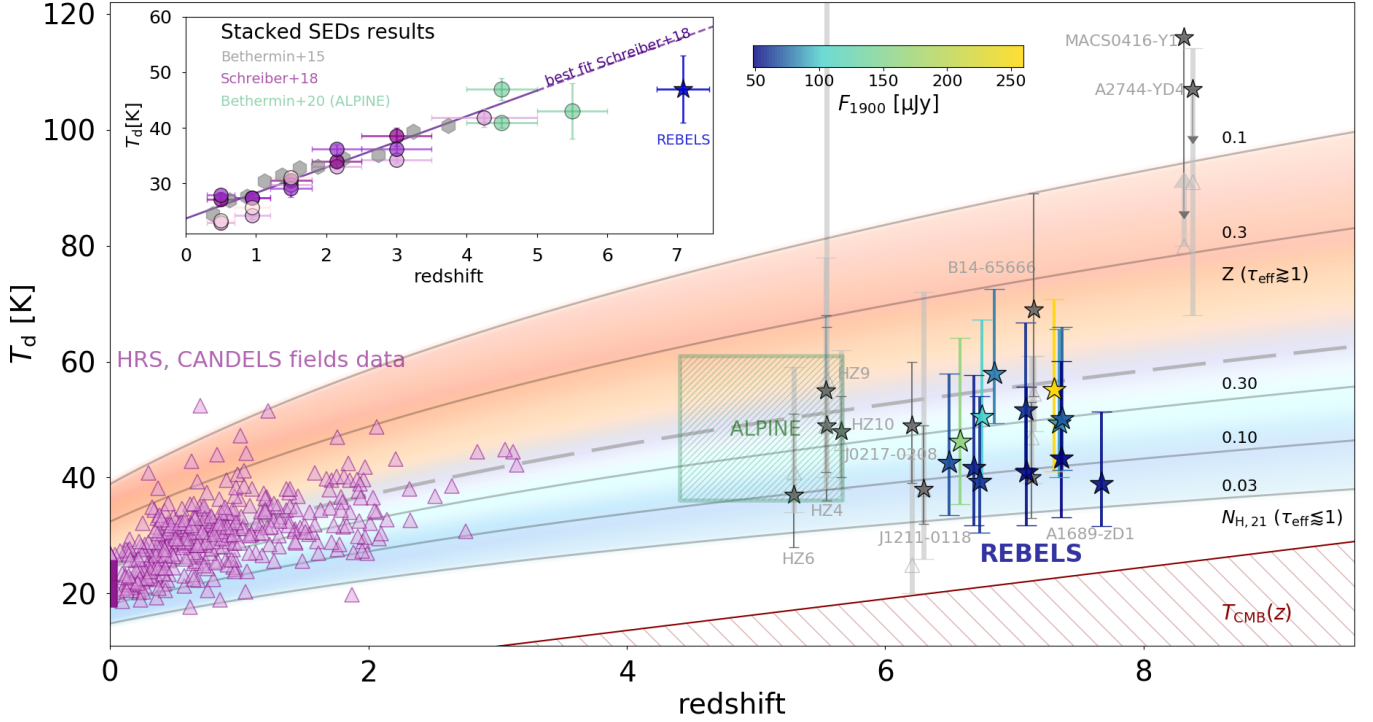


Figure 3. **Main panel:** We unpack the low- z stacked SEDs into the single detections (purple triangles). These are the UV-to-IR normal star forming galaxies detected in the HRS and CANDELS fields (Schreiber et al. 2018). We add the individual UV-selected galaxies at $z \lesssim 5$ for which T_d estimates are available (see Table B1 for the sources details and references). We also show the T_d values obtained with our method for REBELS and ALPINE continuum detected galaxies (respectively, stars and green hatched rectangle). REBELS galaxies are colour-coded according to their F_{1900} (see colorbar). The coloured region shows the T_d -redshift evolution that we derive analytically in eq. 10-18 (for an increasing effective optical depth τ_{eff} from blue to red). We find that on average T_d raises with redshift due to the decreasing gas depletion time at higher- z , as $T_d(z) \propto t_{\text{dep}}^{-1/6}$. The grey dashed line represents the relation given in eq. 10 which can be written explicitly as $T_d = 24.5 (1 + 1.5 z)^{1/6} [\Omega_m(1+z)^3 + \Omega_\Lambda]^{1/12}$ assuming (τ_{eff}, Z) equal unity. We can also explain the scatter in measured T_d at a given redshift. In the UV-transparent approximation ($\tau_{\text{eff}} \lesssim 1$) the scatter depends solely on the column density $N_{\text{H},21} = N_{\text{H}}/10^{21} \text{ cm}^{-2}$ (see solid lines and associated labels). In the UV-obscured approximation ($\tau_{\text{eff}} \gtrsim 1$) the scatter depends only on the metallicity Z (see solid lines and associated labels; note that Z is in solar units). **Inset panel:** T_d values obtained from stacked SEDs fitting in the redshift range $0 \lesssim z \lesssim 6$ (grey, purple and green points, from Béthermin et al. 2015; Schreiber et al. 2018; Béthermin et al. 2020, respectively). The purple line shows the linear best fit obtained by Schreiber et al. (2018) at $z \lesssim 4$. The blue star corresponds to the average temperature $T_d = (47 \pm 6) \text{ K}$ derived here for the REBELS galaxies.

In the previous equation, τ_{eff} is the galaxy effective dust attenuation optical depth at 1500 \AA , which directly relates to the transmissivity, $\tau_{\text{eff}} = -\ln T$. The transmissivity is defined as the ratio of the observed-to-intrinsic UV luminosity, i.e. $T = 1$ ($T = 0$) for a fully transparent (obscured) galaxy. Note that, depending on the relative dust and star distributions, τ_{eff} might significantly differ from the physical UV optical depth, τ_{1500} . Hence, a large transmissivity does not directly imply a low physical optical depth. The conversion factor for (a) continuous star formation at a fix age of 150 Myr , (b) Salpeter IMF in the range $1-100 M_\odot$, (c) metallicity $Z = 1/3 Z_\odot$ is $\mathcal{K}_{1500} \equiv L_{1500}/\text{SFR} = 1.174 \times 10^{10} L_\odot/(M_\odot \text{ yr}^{-1})$ (Ferrara & al., in prep. 2022).

Combining eq. 7 and 9, and recalling that $M_d = DM_g$, it follows that

$$T_d = 29.7 \left[\frac{(1 - e^{-\tau_{\text{eff}}})}{Z} \left(\frac{\text{Gyr}}{t_{\text{dep}}} \right) \right]^{1/(4+\beta_d)} \text{ K} \quad (10)$$

where $\beta_d = 2.03$ and Z is in solar units. We have introduced the *total* gas depletion time $t_{\text{dep}} = M_g/\text{SFR}$, which we derive in the following from cosmological arguments. Eq. 10 shows

that the dust temperature is larger in optically thick, low metallicity systems with a short depletion time.

Let us express M_g and SFR of a galaxy in terms of its total (dark + baryonic) halo mass, M , and mean dark matter accretion rate, $\langle dM/dt \rangle$:

$$M_g = f_b M - M_\star \quad (11)$$

$$\text{SFR} = \epsilon_\star f_b \left\langle \frac{dM}{dt} \right\rangle \quad (12)$$

where ϵ_\star is the star formation efficiency, and $f_b = \Omega_B/\Omega_M$ is the (cosmological) baryon fraction in the halo. By integrating eq. 12 and substituting it into eq. 11 we obtain

$$M_g = f_b M (1 - \epsilon_\star) \quad (13)$$

Numerical simulations (Fakhouri et al. 2010; Dekel & Krumholz 2013; Correa et al. 2015) provide the following fit to the mean halo accretion rate, as a function of redshift and halo mass, $M_{12} = M/10^{12} M_\odot$,

$$\left\langle \frac{dM}{dt} \right\rangle = 69.3 M_{12} f'(z) E(z) M_\odot \text{ yr}^{-1}, \quad (14)$$

with

$$f'(z) = -0.24 + 0.75(1+z); \quad E(z) = [\Omega_m(1+z)^3 + \Omega_\Lambda]^{1/2}. \quad (15)$$

By combining the previous equations t_{dep} takes the form

$$t_{\text{dep}}(z) = t_{\text{d},0} [f'(z)E(z)]^{-1}, \quad (16)$$

where the timescale $t_{\text{d},0} = 14.4(1 - \epsilon_\star)/\epsilon_\star$ Gyr is fixed so that $t_{\text{dep}}(z=0) = 2$ Gyr as approximately measured in local galaxies, including the MW (Bigiel et al. 2008; Leroy et al. 2008; Genzel et al. 2010).

According to eq. 16, the depletion time decreases with redshift as $(1+z)^{-5/2}$ as a result of the higher cosmological accretion rate at early times¹⁴. This point is crucial as, barring variations of the optical depth and metallicity (see below), the redshift evolution of T_{d} is governed by the gas depletion time in galaxies. From the result above, and using eq. 10, it follows that

$$T_{\text{d}} \propto (1+z)^{5/2(4+\beta_{\text{d}})} \approx (1+z)^{0.42}. \quad (17)$$

As we will see shortly, this trend matches perfectly the observed one.

On top of the above overall increasing trend of dust temperature, at fixed redshift scatter is introduced by variations of τ_{eff} and Z in individual galaxies. It is useful to separately discuss two asymptotic regimes, i.e. the optically thin ($1 - e^{-\tau_{\text{eff}}} \approx \tau_{\text{eff}}$), and optically thick ($1 - e^{-\tau_{\text{eff}}} \approx 1$) one. In these two limits eq. 10 becomes

$$\begin{cases} T_{\text{d}} = 29.4 [N_{\text{H},21} f'(z) E(z)]^{1/6.03} \text{ K} & \tau_{\text{eff}} \lesssim 1 (T \gtrsim 37\%), \\ T_{\text{d}} = 29.6 \left[\frac{f'(z) E(z)}{Z} \right]^{1/6.03} \text{ K} & \tau_{\text{eff}} \gtrsim 1 (T \lesssim 37\%); \end{cases} \quad (18)$$

we have used eq. 3 to write $\tau_{\text{eff}}/Z = \sigma_{\text{ext}} N_{\text{H}}$, where $N_{\text{H}} = 10^{21} N_{\text{H},21} \text{ cm}^{-2}$ is the effective gas column density¹⁵ of the galaxy, and $\sigma_{\text{ext}} = 0.96 \times 10^{-21} \text{ cm}^2$ is the extinction cross-section appropriate for the adopted dust model. Eq. 18 is graphically displayed in Fig. 3, where it is also compared with available data.

Interpreting eq. 18 is straightforward. First, for optically thin galaxies (for which UV transmissivity $T \gtrsim 37\%$) T_{d} depends solely on N_{H} , with larger column densities producing warmer dust. Quantitatively, for a $z=0$ source with $N_{\text{H},21} = 1$, corresponding to a ratio $\tau_{\text{eff}}/Z = 0.96$, we predict $T_{\text{d}} = 26.5$ K. Second, dust in obscured sources (for which $T \lesssim 37\%$) is warmer; this is not surprising, as a larger obscuration results in more efficient dust heating. Third, among obscured sources, T_{d} is higher in metal-poor systems. This is because

¹⁴ While t_{dep} is fundamentally unknown at high- z , the *molecular* gas depletion time, $t_{\text{dep,H}_2} = M_{\text{H}_2}/\text{SFR}$, has been studied up to $z \lesssim 5$ via CO and dust observations (see e.g. Tacconi et al. 2018; Walter et al. 2020; Tacconi et al. 2020). For instance, Tacconi et al. (2020) suggest a mild evolution of $t_{\text{dep,H}_2}$ time with redshift for main-sequence galaxies, $t_{\text{dep,H}_2} \propto (1+z)^{-0.98 \pm 0.1}$. Assuming such $t_{\text{dep,H}_2}(z)$ evolution (instead of the one given in eq. 16), does not qualitatively affect our results. In fact, T_{d} would still increase with redshift due to the shorter depletion times. However, the different evolution slightly modifies the predicted $(N_{\text{H},21}, Z)$ values shown in the Figure.

¹⁵ As in general, $\tau_{\text{eff}} < \tau_{1500}$, N_{H} should be intended as a lower limit to the actual mean column density in the galaxy.

a lower metallicity implies a smaller dust content, which for fixed L_{IR} results in warmer temperatures.

Locally, given the observed (N_{H}, Z) scatter in individual sources, our model predicts variations as large as $\Delta T_{\text{d}} \approx 25$ K. We finally note that, if the (N_{H}, Z) range does not evolve with time, the scatter at $z=0$ gets amplified at earlier times by the redshift dependence of T_{d} , reaching $\Delta T_{\text{d}} \approx 55$ K at $z=8$.

4.2 Comparison with observations at $0 \lesssim z \lesssim 8$

We now intend to compare our theoretical predictions with dust temperature estimates available in the literature for UV-detected sources at $0 \lesssim z \lesssim 8$.

We recover the dust temperatures of individual UV-to-IR detected galaxies whose stacked SEDs in the redshift range $0 \lesssim z \lesssim 3$ are used in the analysis by Schreiber et al. (2018). We then add all the UV-selected galaxies at $z \gtrsim 5$ for which dust temperature estimates are available in the literature (see Table B1 for details of the sources). We apply the method used here to derive T_{d} for these galaxies, finding values consistent (within $1 - \sigma$) with SED fitting results (see Table B1 for the detailed comparison). Finally, we apply our method to individual ALPINE galaxies detected simultaneously in [C II] and continuum. We find their median dust temperatures to vary in the range $35 \text{ K} \lesssim T_{\text{d}} \lesssim 60 \text{ K}$, which is consistent with the stacked SEDs fitting results in Bethermin et al. (2020) ($40 \text{ K} \leq T_{\text{d}} \leq 49 \text{ K}$). A detailed analysis of ALPINE galaxies will be presented in Sommovigo & al., in prep. (2022).

The complete collection of T_{d} values is shown in Fig. 3 as a function of redshift. We stress that we consistently compare dust temperatures obtained by fitting individual galaxy SEDs; moreover, the same method is applied to *all* high- z sources (see Appendix B). This avoids the confusion arising from comparing intrinsically different quantities such as dust temperatures obtained from stacked SEDs, and/or peak dust temperatures $T_{\text{peak}} \sim 2.9 \times 10^3 (\lambda_{\text{peak}}/\mu\text{m})^{-1}$.

The physical interpretation of T_{peak} might be unclear for $z > 5$ galaxies. Indeed currently available data at these redshifts hardly trace the peak of FIR emission. Moreover, when a different SED fitting function other than the optically thin grey-body is used, T_{peak} can significantly differ from T_{d} . In fact the assumptions made for the MIR (rest-frame) portion of the spectra affect T_{peak} (Faisst et al. 2020), and the validity of such assumptions cannot be tested as no currently available instrument probes MIR wavelengths at $z > 5$.

We find that our predictions are in agreement with data. Fitting all the dust temperatures with a single power law: $T_{\text{d}}(z) = az^\alpha + b$, we find $\alpha = (0.58 \pm 0.04)$, which is close to the value 0.42 given in eq. 17. The slight difference is due to the fact that T_{d} does not depend uniquely on redshift, as discussed in detail in the previous section (see eq. 18). Hence fitting all the data with a single power-law is misleading.

The additional dependence on the column density (for optically thin sources), and metallicity (for optically thick sources) is responsible for the scatter in the measured temperatures at a given redshift. At $z \approx 0.3$ variations as large as $\Delta T_{\text{d}} = 22$ K are observed (Schreiber et al. 2018), which is perfectly consistent with our predictions ($\Delta T_{\text{d}} \approx 25$ K in the local Universe).

The amplification of the dust temperature scatter at high- z that we predict (if the N_{H}, Z range does not evolve) is also consistent with data. In the narrow redshift range $7.6 \lesssim z \lesssim 8.3$

variations as large as $\Delta T_d = 53$ K are observed (we predicted $\Delta T_d \simeq 55$ K at $z = 8$).

At one extreme there are galaxies hosting very hot dust such as MACS0416-Y1 and A2744-YD4 ($T_d > 80$ K Bakx et al. 2020, and $T_d = 90 \pm 20$ K Laporte et al. 2017; Behrens et al. 2018, respectively). On the other, there are galaxies such as REBELS-18 and J1211-0118 that show more moderate dust temperatures, possibly closer to local sources ($T_d = 39^{+12}_{-7}$ K and $T_d = 38^{+16}_{-8}$ Inoue et al. 2020, respectively).

Our physical model suggests that MACS0416-Y1 and A2744-YD4 are more heavily obscured than most currently observed high- z galaxies. Larger $\tau_{\text{eff}} > 1$ combined with low metallicities $Z/Z_\odot \lesssim 0.3$ can explain the very hot dust temperatures found in these two galaxies.

We explain the colder dust temperatures found in REBELS-18 and J1211-0118 with lower effective optical depths $\tau_{\text{eff}} < 1$, i.e. larger UV transmissivity (ultimately resulting in less efficient dust heating). For these galaxies we predict mean gas column densities around $0.3 \times 10^{20} \text{ cm}^{-2} \lesssim N_{\text{H}} \lesssim 1.0 \times 10^{20} \text{ cm}^{-2}$.

5 SUMMARY AND CONCLUSIONS

We have applied a novel method (Sommovigo et al. 2021) to derive the dust temperature to 13 $z \approx 7$ galaxies part of the ALMA Large Program REBELS. Our method combines the continuum and super-imposed [C II] line emission measurements, thus breaking the SED fitting degeneracy between dust mass and temperature. This allows us to constrain T_d from a single-band restframe observation at 1900 GHz, and to derive dust masses, IR luminosities, and the obscured SFR. Moreover, since REBELS targets constitute the first significant sample of continuum detected sources at $z \sim 7$ (for which T_d estimates are available), we can extend the reported T_d -redshift relation (Magdis et al. 2012a; Magnelli et al. 2013; Béthermin et al. 2015; Schreiber et al. 2018; Faisst et al. 2020; Bouwens et al. 2020) into the Epoch of Reionization.

We summarize below our main findings:

- **Dust temperature and mass:** the median T_d values for REBELS galaxies vary in the range 39 – 58 K, with $\sim 35\%$ associated uncertainty. The median dust masses are in the narrow range $(0.9 - 3.6) \times 10^7 M_\odot$. Dust production from SNe alone in most cases (85%) can generate such dust masses assuming a dust yield $\lesssim 1 M_\odot$ per SN;

- **IR luminosities and L_{1900} -to- L_{IR} conversion at $z \sim 7$:** REBELS galaxies IR luminosities vary in the range $1.7 \times 10^{11} L_\odot \lesssim L_{\text{IR}} \lesssim 2.8 \times 10^{12} L_\odot$, which corresponds to obscured SFRs around $\sim 17 - 285 M_\odot/\text{yr}$. We also derive their average conversion factor $L_{\text{IR}} = 14^{+8}_{-3} L_{1900}$, where $L_{1900} = \nu_0 L_{\nu_0}$, with $\nu_0 = 1900$ GHz. This value is consistent with an extrapolation of the empirical fitting formula of Bouwens et al. (2020) to $z \approx 7$;

- **Dust temperature cosmic evolution:** we produce a *new physical model* (see eq. 10-18) that motivates the dust temperature increase with redshift. Such trend is an imprint of the decreasing gas depletion time towards high- z , $t_{\text{dep}} \propto (1+z)^{5/2}$. We show that $T_d \propto t_{\text{dep}}^{-1/6}$, or $T_d \approx (1+z)^{0.42}$;

- **Dust temperature scatter at a given redshift:** on top of the T_d - z trend, we can also physically motivate the scatter in the measured T_d values at a given redshift. We find that in UV-transparent galaxies (UV transmissivity $\gtrsim 37\%$) the scatter

in T_d depends solely on the column density N_{H} , with larger N_{H} corresponding to hotter dust. Instead, in UV-obscured galaxies the scatter in T_d depends only on the metallicity Z , with lower Z implying hotter dust.

A very hot dust component, implying a large obscured SFR, can coexist with a steep UV slope in the presence of *spatial segregation* of IR and UV emitting regions. This possibility has been suggested by theoretical studies and simulations in some $z \sim 7 - 8$ sources (Behrens et al. 2018; Liang et al. 2019; Sommovigo et al. 2020). Such scenario is also supported by some observations; for instance Hodge et al. (2012, 2016); Carniani et al. (2017); Laporte et al. (2017); Bowler et al. (2018, 2021) find significant spatial offset between their ALMA and HST data. High-resolution ALMA follow-up observations of REBELS galaxies are required in order to make a step forward (see also Inami & al., in prep. 2022; Ferrara & al., in prep. 2022 for a discussion on this point).

JWST will also provide us with much more accurate metallicity measurements at $z \gtrsim 5$, improving current estimates of the dust-to-gas ratios at high- z . Finally, further ALMA observation at shorter wavelengths in band 7 – 8 – 9, will allow us to reduce the uncertainties in current dust temperatures estimates at $z \gtrsim 5$ by sampling galaxies SEDs closer to the FIR emission peak (see Fig. 1 and the discussion in Bakx et al. 2021).

ACKNOWLEDGEMENTS

LS, AF, AP acknowledge support from the ERC Advanced Grant INTERSTELLAR H2020/740120 (PI: Ferrara). Any dissemination of results must indicate that it reflects only the author’s view and that the Commission is not responsible for any use that may be made of the information it contains. Partial support from the Carl Friedrich von Siemens-Forschungspreis der Alexander von Humboldt-Stiftung Research Award is kindly acknowledged (AF). PD acknowledges support from the ERC starting grant DELPHI StG-717001, from the NWO grant ODIN 016.VIDI.189.162 and the European Commission’s and University of Groningen’s CO-FUND Rosalind Franklin program. RJB and MS acknowledge support from TOP grant TOP1.16.057. SS acknowledges support from the Nederlandse Onderzoekschool voor Astronomie (NOVA). RS and RAB acknowledge support from STFC Ernest Rutherford Fellowships [grant numbers ST/S004831/1 and ST/T003596/1]. RE acknowledges funding from JWST/NIRCam contract to the University of Arizona, NAS5-02015. PAO, LB, and YF acknowledge support from the Swiss National Science Foundation through the SNSF Professorship grant 190079 “Galaxy Build-up at Cosmic Dawn”. HI and HSBA acknowledge support from the NAOJ ALMA Scientific Research Grant Code 2021-19A. HI acknowledges support from the JSPS KAKENHI Grant Number JP19K23462. JH gratefully acknowledges support of the VIDI research program with project number 639.042.611, which is (partly) financed by the Netherlands Organisation for Scientific Research (NWO). MA acknowledges support from FONDECYT grant 1211951, “ANID+PCI+INSTITUTO MAX PLANCK DE ASTRONOMIA MPG 190030”, “ANID+PCI+REDES 190194” and ANID BASAL project FB210003. LG and RS acknowledge support from the Amaldi Research Center

funded by the MIUR program “Dipartimento di Eccellenza” (CUP:B81I18001170001). YF further acknowledges support from NAOJ ALMA Scientific Research Grant number 2020-16B “ALMA HzFINEST: High-z Far-Infrared Nebular Emission Studies”. IDL acknowledges support from ERC starting grant DustOrigin 851622. JW acknowledges support from the ERC Advanced Grant QUENCH 695671, and from the Fondation MERAC. EdC gratefully acknowledges support from the Australian Research Council Centre of Excellence for All Sky Astrophysics in 3 Dimensions (ASTRO 3D), through project number CE170100013.

DATA AVAILABILITY

Data generated in this research will be shared on reasonable request to the corresponding author.

REFERENCES

- Aoyama S., Hou K.-C., Shimizu I., Hirashita H., Todoroki K., Choi J.-H., Nagamine K., 2017, *MNRAS*, **466**, 105
- Atek H., et al., 2015, *Astrophysical Journal*, 814
- Bakx T. J. L. C., et al., 2020, *MNRAS*, **493**, 4294
- Bakx T. J. L. C., et al., 2021, arXiv e-prints, p. arXiv:2108.13479
- Barisic I., et al., 2017, *The Astrophysical Journal*, 845, 41
- Behrens C., Pallottini A., Ferrara A., Gallerani S., Vallini L., 2018, *MNRAS*, **477**, 552
- B  thermin M., et al., 2015, *A&A*, **573**, A113
- B  thermin M., et al., 2020, arXiv e-prints, p. arXiv:2002.00962
- Bigiel F., Leroy A., Walter F., Brinks E., de Blok W. J. G., Madore B., Thornley M. D., 2008, *AJ*, **136**, 2846
- Blain A. W., Barnard V. E., Chapman S. C., 2003, *Monthly Notices of the Royal Astronomical Society*, 338, 733
- Bocchio M., Marassi S., Schneider R., Bianchi S., Limongi M., Chieffi A., 2016, *A&A*, **587**, A157
- Bouwens R. J., et al., 2010, *ApJL*, **709**, L133
- Bouwens R. J., et al., 2011, *Nature*, **469**, 504
- Bouwens R. J., et al., 2015, *ApJ*, **803**, 34
- Bouwens R. J., et al., 2016, *ApJ*, **833**, 72
- Bouwens R., et al., 2020, *ApJ*, **902**, 112
- Bouwens R. J., et al., 2021, arXiv e-prints, p. arXiv:2106.13719
- Bowler R. A. A., et al., 2015, *MNRAS*, **452**, 1817
- Bowler R. A. A., Dunlop J. S., McLure R. J., McLeod D. J., 2017, *MNRAS*, **466**, 3612
- Bowler R. A. A., Bourne N., Dunlop J. S., McLure R. J., McLeod D. J., 2018, *MNRAS*, **481**, 1631
- Bowler R. A. A., Cullen F., McLure R. J., Dunlop J. S., Avison A., 2021, *MNRAS*,
- Bradley L. D., et al., 2012, *ApJ*, **760**, 108
- Bradley L. D., et al., 2014, *ApJ*, **792**, 76
- Calzetti D., Armus L., Bohlin R. C., Kinney A. L., Koornneef J., Storchi-Bergmann T., 2000, *The Astrophysical Journal*, 533, 682
- Capak P., et al., 2015, *Nature*, 522, 455
- Carilli C. L., Walter F., 2013, *ARA&A*, **51**, 105
- Carilli C. L., et al., 2016, *The Astrophysical Journal*, 833, 73
- Carniani S., et al., 2017, *A&A*, **605**, A42
- Carniani S., et al., 2018, *MNRAS*, **478**, 1170
- Carniani S., et al., 2020, arXiv e-prints, p. arXiv:2006.09402
- Casey C. M., 2012, *MNRAS*, **425**, 3094
- Casey C. M., Hodge J., Zavala J. A., Spilker J., da Cunha E., Staguhn J., Finkelstein S. L., Drew P., 2018, *The Astrophysical Journal*, 862, 78
- Chabrier G., 2003, *ApJL*, **586**, L133
- Chevallard J., Charlot S., 2016, *Monthly Notices of the Royal Astronomical Society*, 462, 1415
- Chevallard J., et al., 2019, *MNRAS*, **483**, 2621
- Correa C. A., Wyithe J. S. B., Schaye J., Duffy A. R., 2015, *MNRAS*, **450**, 1521
- Daddi E., et al., 2010, *The Astrophysical Journal*, 714, L118
- Dale D. A., et al., 2012, *The Astrophysical Journal*, 745, 95
- Dayal P., Ferrara A., 2018, *Phys. Rep.*, **780**, 1
- Dayal P., al., in prep. 2022, 0, 0
- Dayal P., Dunlop J. S., Maio U., Ciardi B., 2013, *MNRAS*, **434**, 1486
- De Breuck C., et al., 2019, *A&A*, 631, A167
- De Looze I., et al., 2014, *A&A*, **568**, A62
- Dekel A., Krumholz M. R., 2013, *Monthly Notices of the Royal Astronomical Society*, 432, 455
- Draine B., 1989, in *Infrared spectroscopy in astronomy*.
- Draine B., 2003, *Annual Review of Astronomy and Astrophysics*, 41, 241
- Draine B. T., Li A., 2007, *ApJ*, **657**, 810
- Dunlop J. S., 2016, *The Messenger*, **166**, 48
- Dunlop J. S., et al., 2013, *Monthly Notices of the Royal Astronomical Society*, 432, 3520
- Dunne L., Eales S. A., 2001, *Monthly Notices of the Royal Astronomical Society*, 327, 697
- Ellis R. S., et al., 2012, *The Astrophysical Journal*, 763, L7
- Faisst A. L., Fudamoto Y., Oesch P. A., Scoville N., Riechers D. A., Pavesi R., Capak P., 2020, arXiv e-prints, p. arXiv:2005.07716
- Fakhouri O., Ma C.-P., Boylan-Kolchin M., 2010, *Monthly Notices of the Royal Astronomical Society*, 406, 2267
- Ferrara A., Tolstoy E., 2000, *Monthly Notices of the Royal Astronomical Society*, 313, 291
- Ferrara A., al., in prep. 2022, 0, 0
- Ferrara A., Vallini L., Pallottini A., Gallerani S., Carniani S., Khandel M., Decataldo D., Behrens C., 2019, *Monthly Notices of the Royal Astronomical Society*, 489, 1
- Fudamoto Y., et al., 2020, *MNRAS*, **491**, 4724
- Fudamoto Y., et al., 2021, *Nature*, 597, 489–492
- Fujimoto S., et al., 2019, *ApJ*, **887**, 107
- Fujimoto S., et al., 2020, arXiv e-prints, p. arXiv:2003.00013
- Galametz M., et al., 2012, *Monthly Notices of the Royal Astronomical Society*, 425, 763
- Galliano F., Dwek E., Chaniai P., 2008, *ApJ*, **672**, 214
- Genzel R., et al., 2010, *MNRAS*, **407**, 2091
- Ginolfi M., et al., 2020, *A&A*, **633**, A90
- Graziani L., Schneider R., Ginolfi M., Hunt L. K., Maio U., Glatzle M., Ciardi B., 2020, *MNRAS*, **494**, 1071
- Harikane Y., et al., 2020, *ApJ*, **896**, 93
- Hashimoto T., et al., 2018, *Nature*, **557**, 392
- Hashimoto T., et al., 2019, *Pub. Astron. Soc. Japan*, **71**, 71
- Heiderman A., Evans N. J., Allen L. E., Huard T., Heyer M., 2010, *The Astrophysical Journal*, 723, 1019
- Hildebrand R. H., 1983, *QJRAS*, **24**, 267
- Hodge J. A., da Cunha E., 2020, *Royal Society Open Science*, **7**, 200556
- Hodge J. A., Carilli C. L., Walter F., de Blok W. J. G., Riechers D., Daddi E., Lentati L., 2012, *ApJ*, **760**, 11
- Hodge J. A., et al., 2016, *ApJ*, **833**, 103
- Hollenbach D. J., Tielens A. G. G. M., 1999, *Rev. Mod. Phys.*, **71**, 173
- Hygate A., al., in prep. 2022, 0, 0
- Inami H., al., in prep. 2022, 0, 0
- Inoue A. K., et al., 2016, *Science*, **352**, 1559
- Inoue A. K., Hashimoto T., Chihara H., Koike C., 2020, *Monthly Notices of the Royal Astronomical Society*, 495, 1577
- James A., Dunne L., Eales S., Edmunds M. G., 2002, *MNRAS*, **335**, 753
- Jones T., Sanders R., Roberts-Borsani G., Ellis R. S., Laporte N., Treu T., Harikane Y., 2020, arXiv e-prints, p. arXiv:2006.02447

- Kennicutt Robert C. J., 1998, *ApJ*, **498**, 541
- Kirkpatrick A., et al., 2012, *The Astrophysical Journal*, 759, 139
- Knudsen K. K., Richard J., Kneib J.-P., Jauzac M., Clément B., Drouart G., Egami E., Lindroos L., 2016a, *Monthly Notices of the Royal Astronomical Society: Letters*, 462, L6
- Knudsen K. K., Watson D., Frayer D., Christensen L., Gallazzi A., Michałowski M. J., Richard J., Zavala J., 2016b, *Monthly Notices of the Royal Astronomical Society*, 466, 138
- Kovács A., et al., 2010, *The Astrophysical Journal*, 717, 29
- Laporte N., et al., 2017, *ApJL*, **837**, L21
- Laporte N., et al., 2019, *Monthly Notices of the Royal Astronomical Society: Letters*, 487, L81
- Leroy A. K., Walter F., Brinks E., Bigiel F., de Blok W. J. G., Madore B., Thornley M. D., 2008, *The Astronomical Journal*, 136, 2782
- Leroy A. K., et al., 2011, *The Astrophysical Journal*, 737, 12
- Leńniewska A., Michałowski M. J., 2019, *Astronomy & Astrophysics*, 624, L13
- Liang L., et al., 2019, *MNRAS*, p. 2072
- Livermore R. C., Finkelstein S. L., Lotz J. M., 2017, *ApJ*, **835**, 113
- Lonsdale C. J., Farrah D., Smith H. E., 2006, *Ultraluminous Infrared Galaxies*. p. 285, doi:10.1007/3-540-30313-8-9
- Ma X., Hopkins P. F., Faucher-Giguère C.-A., Zolman N., Muratov A. L., Kereš D., Quataert E., 2016, *MNRAS*, **456**, 2140
- Ma X., et al., 2019, *MNRAS*, **487**, 1844
- Magdis G. E., et al., 2012a, *ApJ*, **760**, 6
- Magdis G. E., et al., 2012b, *ApJ*, **760**, 6
- Magnelli B., et al., 2013, *A&A*, **553**, A132
- Magnelli B., et al., 2014, *A&A*, **561**, A86
- Maiolino R., Mannucci F., 2019, *The Astronomy and Astrophysics Review*, 27
- Mancini M., Schneider R., Graziani L., Valiante R., Dayal P., Maio U., Ciardi B., Hunt L. K., 2015, *MNRAS*, **451**, L70
- Matsuura M., et al., 2019, *MNRAS*, **482**, 1715
- Matthee J., et al., 2017, *The Astrophysical Journal*, 851, 145
- Matthee J., et al., 2019, *The Astrophysical Journal*, 881, 124
- McLure R. J., et al., 2013, *MNRAS*, **432**, 2696
- Meurer G. R., Heckman T. M., Calzetti D., 1999, *The Astrophysical Journal*, 521, 64
- Michałowski M. J., 2015, *A&A*, **577**, A80
- Novikov I. D., et al., 2021, *Physics-Uspekhi*, 64, 386
- Oesch P. A., et al., 2013, *The Astrophysical Journal*, 773, 75
- Oesch P. A., et al., 2016, *The Astrophysical Journal*, 819, 129
- Pallottini A., et al., 2019, *MNRAS*, **487**, 1689
- Pallottini A., et al., 2022, arXiv e-prints, p. arXiv:2201.02636
- Pavesi R., et al., 2016a, *ApJ*, **832**, 151
- Pavesi R., et al., 2016b, *The Astrophysical Journal*, 832, 151
- Pavesi R., Riechers D. A., Faisst A. L., Stacey G. J., Capak P. L., 2019, *ApJ*, **882**, 168
- Pereira-Santaella M., Rigopoulou D., Farrah D., Leboutteiller V., Li J., 2017, *Monthly Notices of the Royal Astronomical Society*, 470, 1218
- Planck Collaboration et al., 2016, *A&A*, **596**, A107
- Rémy-Ruyer A., et al., 2014, *A&A*, **563**, A31
- Reuter C., et al., 2020, arXiv e-prints, p. arXiv:2006.14060
- Rybak M., et al., 2019, *ApJ*, **876**, 112
- Santini P., et al., 2017, *The Astrophysical Journal*, 847, 76
- Schaerer D., et al., 2020, arXiv e-prints, p. arXiv:2002.00979
- Schouws S., al., in prep. 2022, 0, 0
- Schouws S., et al., 2021, arXiv e-prints, p. arXiv:2105.12133
- Schreiber C., Elbaz D., Pannella M., Ciesla L., Wang T., Franco M., 2018, *A&A*, **609**, A30
- Shen X., Vogelsberger M., Nelson D., Tacchella S., Hernquist L., Springel V., Marinacci F., Torrey P., 2021, arXiv e-prints, p. arXiv:2104.12788
- Slavin J. D., Dwek E., Mac Low M.-M., Hill A. S., 2020, *ApJ*, **902**, 135
- Sommovigo L., al., in prep. 2022, 0, 0
- Sommovigo L., Ferrara A., Pallottini A., Carniani S., Gallerani S., Decataldo D., 2020, arXiv e-prints, p. arXiv:2004.09528
- Sommovigo L., Ferrara A., Carniani S., Zanella A., Pallottini A., Gallerani S., Vallini L., 2021, arXiv e-prints, p. arXiv:2102.08950
- Stacey G. J., Geis N., Genzel R., Lugten J. B., Poglitsch A., Sternberg A., Townes C. H., 1991, *ApJ*, **373**, 423
- Stark D. P., 2016, *Annual Review of Astronomy and Astrophysics*, 54, 761
- Stefanon L., al., in prep. 2022, 0, 0
- Tacconi L. J., et al., 2018, *ApJ*, **853**, 179
- Tacconi L. J., Genzel R., Sternberg A., 2020, *ARA&A*, **58**, 157
- Tamura Y., et al., 2019, *ApJ*, **874**, 27
- Tomczak A. R., et al., 2016, *The Astrophysical Journal*, 817, 118
- Topping M., al., in prep. 2022, 0, 0
- Torrey P., et al., 2019, *MNRAS*, **484**, 5587
- Vallini L., Ferrara A., Pallottini A., Carniani S., Gallerani S., 2020, *MNRAS*,
- Vallini L., Ferrara A., Pallottini A., Carniani S., Gallerani S., 2021, *MNRAS*, **505**, 5543
- Walter F., et al., 2020, arXiv e-prints, p. arXiv:2009.11126
- Watson D., Christensen L., Knudsen K. K., Richard J., Gallazzi A., Michałowski M. J., 2015, *Nature*, **519**, 327
- Weingartner J. C., Draine B., 2001, *The Astrophysical Journal*, 548, 296
- Wiedner M. C., et al., 2021, *Experimental Astronomy*,
- Wolfire M. G., McKee C. F., Hollenbach D., Tielens A. G. G. M., 2003, *The Astrophysical Journal*, 587, 278
- Wright S. A., Law D. R., Ellis R. S., Erb D. K., Larkin J. E., Lu J. R., Steidel C. C., 2010, *The Astronomy and Astrophysical Decadal Survey*, Science White paper
- Zanella A., et al., 2018, *MNRAS*, **481**, 1976
- da Cunha E., Charlot S., Elbaz D., 2008, *MNRAS*, **388**, 1595
- da Cunha E., et al., 2015, *The Astrophysical Journal*, 806, 110

APPENDIX A: INDIVIDUAL SEDS

In Fig. B1 we show the individual FIR SEDs obtained for all REBELS [C II] and continuum detected galaxies (analogously to the central panel in Fig. 1 representing REBELS-12 only). For all the sources we show the SEDs obtained with their median values of (T_d, M_d) , and the variation due to the $1\text{-}\sigma$ uncertainties in these two quantities (on average $\Delta T_d/T_d \sim 30\%$ and $\Delta M_d/M_d = 70\%$).

These large uncertainties result from the lack of information on the metallicity Z and burstiness parameter κ_s of REBELS galaxies (see the discussion in Section 3). Future observations will help us to constrain both these quantities, thus reducing the uncertainties in the predicted T_d, M_d . In fact, with ALMA we can investigate the [O III]/[C II] luminosities ratios of REBELS sources, which can be used to reliably constrain their κ_s using the model in Vallini et al. 2021 (these ALMA observations would also provide us with an additional data point in the FIR continuum underlying [O III]). Moreover, future JWST optical nebular lines observations will allow us to improve metallicity estimates out to very high- z , possibly reaching a precision as low as $\Delta Z/Z \sim 35\%$ at $z \sim 7$ (Wright et al. 2010; Chevillard et al. 2019; Maiolino & Mannucci 2019).

APPENDIX B: APPLICATION TO OTHER SAMPLES

In Table B1 we show the comparison between measured dust temperatures for galaxies at $z > 5$ available in the literature compared with the results from our method. Here we briefly discuss the assumptions used in our derivation.

For the galaxies MACS0416-Y1, B14-65666 and A1689-zD1 we refer to the dedicated works discussing the application of our method in comparison to multiple-band SED fitting¹⁶ (MACS0416-Y1, B14-65666: Sommovigo et al. 2021, A1689-zD1: Bakx et al. 2021). We highlight that A1689-zD1 is the only $z > 5$ galaxy for which a band-9 continuum detection, short-wards of the peak of FIR emission, is available. It is very promising that also in this case -where traditional SED fitting is particularly precise thanks to the widespread continuum data available- our method gives a consistent T_d value (within $\sim 0.5 \sigma$).

For the remaining sources detected in both [O III]88 μm and [C II]158 μm (all but HZ4-10), Vallini et al. (2021) derived the value of (κ_s, Z) , albeit with large uncertainties (on average: $10 \lesssim \kappa_s \lesssim 80$ and $0.2 \lesssim Z/Z_\odot \lesssim 0.4$; see Table 1 in the paper). For each individual source we assume a random distribution for (κ_s, Z) around the mean value, with the dispersion corresponding to the uncertainty. For all of these sources the ratio $y = r_{\text{CII}}/r_{\text{star}}$ is also measured: $y = 1.8 \pm 0.4$ (J1211-0118 and J0217-0208, Harikane et al. 2020), $y = 8 \pm 2$ (A2744-YD4, Laporte et al. 2019). Finally, for HZ4-10, due to the lack of observational constraints on (Z, κ_s, y) , we rely on the same assumptions used for both the ALPINE individual galaxies and the REBELS galaxies, which are extensively described and motivated in Section 3.

In all cases with our method we derive T_d values consistent with literature estimates well within $\pm 30\%$. The more

Table B1. Measured dust temperatures for galaxies at $z > 5$ available in the literature compared with the results from our method. We note that for the literature data, we always show the result derived from traditional SED fitting in the most recent reference. The only case in which we provide two estimates is that of A2744-YD4, as the latest one is obtained from ad hoc simulations rather than direct measurements (2, Behrens et al. 2018). These temperatures are the ones shown in Fig. 3 as grey triangles (literature data) and stars (our derivations). **References:** 1 (Laporte et al. 2019), 2 (Behrens et al. 2018), 3 (Bakx et al. 2020), 4 (Tamura et al. 2019), 5 (Hashimoto et al. 2019), 6 (Bowler et al. 2018), 7 (Bakx et al. 2021), 8 (Knudsen et al. 2016b), 9 (Watson et al. 2015), 10 (Harikane et al. 2020), 11 (Faisst et al. 2020), 12 (Pavesi et al. 2016b; Pavesi et al. 2019), 13 (Capak et al. 2015).

<i>Derived</i>	ID#	<i>Literature</i>		
T_d [K]		T_d [K]	z	Ref.
< 75	A2744-YD4	> 55	8.38	1
< 107	A2744-YD4	91 ± 23	8.38	2
< 116	MACS0416-Y1	> 80	8.31	3, 4
69^{+20}_{-15}	B14-65666	$48 - 61$	7.15	5, 6
40^{+13}_{-7}	A1689-zD1	47^{+15}_{-9}	7.133	7, 8, 9
38^{+11}_{-6}	J1211-0118	38^{+34}_{-12}	6.0295	10
49^{+11}_{-10}	J0217-0208	25^{+19}_{-5}	6.204	10
48^{+6}_{-8}	HZ10	46^{+16}_{-8}	5.657	11, 12, 13
49^{+17}_{-13}	HZ4	57^{+67}_{-17}	5.544	11, 12, 13
55^{+13}_{-14}	HZ9	49^{+29}_{-11}	5.541	11, 12, 13
37^{+14}_{-8}	HZ6	41^{+18}_{-7}	5.293	11, 12, 13

discrepant case is represented by J0217-0208 for which we predict a warmer temperature, albeit consistent within the large uncertainty given from SED fitting ($\sim 52\%$).

We note that for this galaxy, assuming the dust model adopted here, from traditional SED fitting (relying only on the two detections at 120 μm , 158 μm) one would deduce a very large dust mass $\log(M_d/M_\odot) = 9.28 \pm 0.17$. Given the stellar mass estimated for this galaxy ($M_\star \sim 3 \times 10^{10} M_\odot$ from Harikane et al. 2020), such dust mass would imply a very large dust yield of $y_d = 3^{+2}_{-1} M_\odot$ per SN, which is not compatible with SNe dust production constraints (Bocchio et al. 2016; Matsuura et al. 2019; Leńniewska & Michałowski 2019; Slavin et al. 2020). Further ALMA observations at shorter wavelengths will help us understand whether the dust temperature of this galaxy has been underestimated (and thus the dust mass overestimated), which would reduce the tension with the T_d value derived with our method. An other possibility is that the stellar mass of this source has been underestimated, this would relax the requirements set by the condition on $M_d < M_{d,\text{max}} \propto M_{\text{star}}$ (see Section 2), allowing for larger dust masses and lower temperatures in our derivation. If neither of these possibilities is verified, alternative dust production scenarios might have to be invoked for this source (see the discussion in Section 3.2).

This paper has been typeset from a \LaTeX file prepared by the author.

¹⁶ The minor differences in the quoted T_d values arise from the change in the adopted dust model, see also Section 2

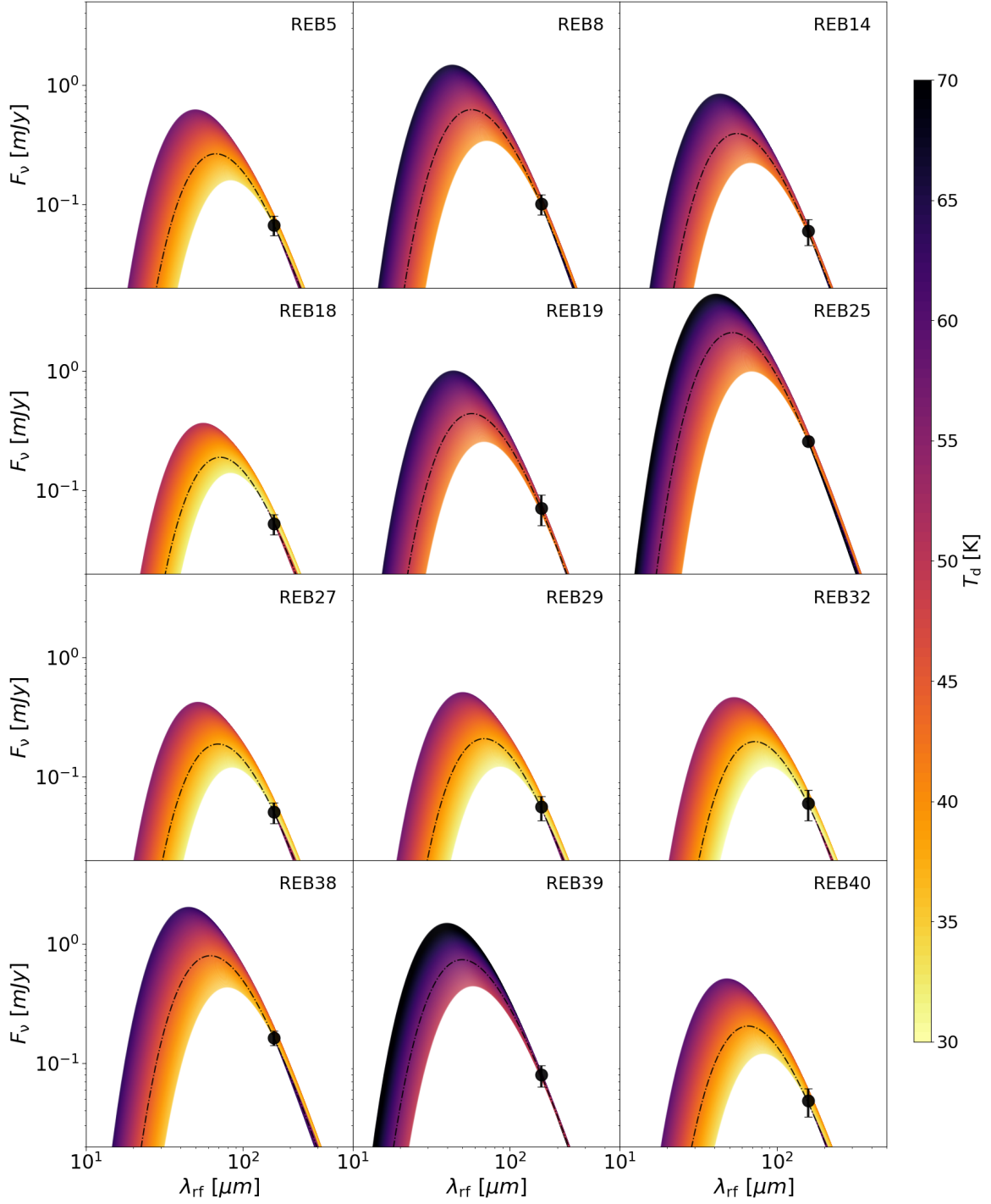


Figure B1. Variation in the derived SEDs of all REBELS [C II] and continuum detected galaxies due to the $1 - \sigma$ uncertainties in their individual (T_d, M_d) . The SEDs are colour coded according to the corresponding dust temperatures (see colorbar). The dashed black curves show the SEDs obtained with the median (T_d, M_d) values for each galaxy. The black points represent the continuum observations at 1900 GHz. For further details on the sources see Table 1).